Period p-tuplings in coupled maps

Sang-Yoon Kim
School of Physics, Georgia Institute of Technology, Atlanta, Georgia 30332-0430
and Department of Physics, Kangwon National University, Chunchon, Kangwon-Do 200-701, Korea
(Received 1 April 1996; revised manuscript received 24 June 1996)

We study the critical behavior (CB) of all period p-tuplings ($p=2,3,4,\ldots$) in N ($N=2,3,4,\ldots$) symmetrically coupled one-dimensional maps. We first investigate the CB for the $N=2$ case of two-coupled maps, using a renormalization method. Three (five) kinds of fixed points of the renormalization transformation and their relevant ''coupling eigenvalues'' associated with coupling perturbations are found in the case of even (odd) p. We next study the CB for the linear- and nonlinear-coupling cases (a coupling is called linear or nonlinear according to its leading term), and confirm the renormalization results. Both the structure of the critical set (set of the critical points) and the CB vary according to whether the coupling is linear or nonlinear. Finally, the results of the two-coupled maps are extended to many-coupled maps with $N\geqslant 3$, in which the CB depends on the range of coupling. [S1063-651X(96)02310-0]

PACS number(s): 05.45.+b, 03.20.+i, 05.70.Jk

I. INTRODUCTION

Universal scaling behavior of period p-tuplings ($p=2,3,4,\ldots$) has been found in a one-parameter family $f_A(x)$ of one-dimensional (1D) unimodal maps with a quadratic maximum. As the nonlinearity parameter A increases, a stable fixed point undergoes the cascade of period-doubling bifurcations accumulating at a finite parameter value A_∞. The period-doubling sequence corresponding to the MSS (Metropolis, Stein, and Stein [1]) sequence R^{*n} [for details of the MSS sequences and the $(*)$-composition rule, see Refs. [1,2]] exhibits an asymptotic scaling behavior [3].

What happens beyond the period-doubling accumulation point A_∞ is interesting from the viewpoint of chaos. The parameter interval between A_∞ and the final boundary-crisis point A_c beyond which no periodic or chaotic attractors can be found within the unimodality interval is called the ''chaotic'' regime. Within this region, besides the period-doubling sequence, there are many other sequences of periodic orbits exhibiting their own scaling behavior. In particular, every primary pattern P [that cannot be decomposed using the $(*)$ operation] leads to a MSS sequence P^{*n}. For example, $P=RL$ leads to a period-tripling sequence, $P=RL^2$ to a period-quadrupling sequence, and the three different $P=RLR^2, RL^2R$, and RL^3 to three different period-quintupling sequences. Thus there exist infinitely many higher period p-tupling ($p=3,4,\ldots$) sequences inside the chaotic regime. Unlike the period-doubling sequence, stability regions of periodic orbits in the higher period p-tupling sequences are not adjacent on the parameter axis, because they are created by their own tangent bifurcations. The asymptotic scaling behavior of these (disconnected) higher period p-tupling sequences characterized by the parameter and orbital scaling factors, δ and α, vary depending on the primary pattern P [2,4–10].

In this paper we consider N ($N=2,3,4,\ldots$) symmetrically coupled 1D maps, which may be used as models of coupled nonlinear oscillators such as Josephson-junction arrays or chemically reacting cells, and so on [11]. We are interested in the critical behavior (CB) of period p-tuplings ($p=2,3,\ldots$) in the coupled 1D maps. The period-doubling case with $p=2$ was previously studied [12,13]. Here we study the critical scaling behavior of all the other higher period p-tuplings ($p=3,4,\ldots$).

Using a renormalization method, we first investigate the critical behavior for the $N=2$ case of two-coupled maps in Sec. II. In the case of even (odd) p, we find three (five) kinds of fixed points of a renormalization transformation and their relevant coupling eigenvalues (CE's) associated with coupling perturbations. A short account of the renormalization result has already been published [14]. We next consider two kinds of couplings, linear- and nonlinear-coupling cases; a coupling is called linear or nonlinear according to its leading term. As examples of the linear- and nonlinear-coupling cases, we study the linearly and dissipatively coupled maps, respectively, in Sec. III, and confirm the renormalization results. The structure of the critical set (set of the critical points) varies depending on the nature of coupling. In the linearly coupled case, an infinite number of critical line segments and the zero-coupling critical point, at which the N 1D maps become uncoupled, constitute the critical set, while in the dissipatively coupled case, the critical set consists of only one critical line segment, one end of which is the zero-coupling critical point. The CB also depends on the position on the critical set. For even (odd) p, three (four) kinds of fixed points govern the CB for the linearly coupled case, whereas only two (three) fixed points govern the CB for the dissipatively coupled case.

In Sec. IV we extend the results of the two-coupled maps to many-coupled maps with $N\geqslant 3$. It is found that the critical scaling behavior depends on the range of coupling. In the extreme long-range case of global coupling, in which each 1D map is coupled to all the other 1D maps with equal strength, both the structure of the critical set and the CB are the same as those for the two-coupled case, independently of N. However, for the cases of nonglobal couplings of shorter range, a significant change in the structure of the critical set may or may not occur according to whether the coupling is linear or not. For the case of a linear nonglobal coupling,

only the zero-coupling critical point is left in the parameter plane, which is in contrast to the global-coupling case. On the other hand, for the case of a nonlinear nonglobal coupling, one critical line segment still remains, as in the globally coupled case. Finally, a summary is given in Sec. V.

II. RENORMALIZATION ANALYSIS OF TWO-COUPLED MAPS

In this section we first discuss stability of periodic orbits in two-coupled 1D maps, and then study the CB associated with period p-tuplings ($p=2,3,4,\ldots$) using a renormalization method. Three (five) kinds of fixed points of a renormalization operator and their relevant CE's with moduli larger than unity are found in the case of even (odd) p.

A. Stability of periodic orbits in two-coupled maps

We consider a map T consisting of two symmetrically coupled 1D maps,

$$T:\begin{cases} x_{t+1}=F(x_t,y_t)=f(x_t)+g(x_t,y_t) \\ y_{t+1}=F(y_t,x_t)=f(y_t)+g(y_t,x_t), \end{cases} \tag{2.1}$$

where t denotes a discrete time, $f(x)$ is a 1D unimodal map with a quadratic maximum at $x=0$, and $g(x,y)$ is a coupling function. The uncoupled 1D map f satisfies a normalization condition

$$f(0)=1, \tag{2.2}$$

and the coupling function g obeys a condition

$$g(x,x)=0 \quad \text{for any } x. \tag{2.3}$$

The two-coupled map (2.1) is invariant under the exchange of coordinates such that $x\leftrightarrow y$. The set of all points which are invariant under the exchange of coordinates forms a symmetry line $y=x$. An orbit is called a(n) (in-phase) synchronous orbit if it lies on the symmetry line, i.e., it satisfies

$$x_t=y_t \quad \text{for all } t. \tag{2.4}$$

Otherwise, it is called an (out-of-phase) asynchronous orbit. Here we study only the synchronous orbits, which can be easily found from the uncoupled 1D map, $x_{t+1}=f(x_t)$, because of the condition (2.3).

Stability analysis of a periodic orbit in the two-coupled map T can be conveniently carried out in a set of new coordinates (X,Y), defined by

$$X=\frac{(x+y)}{2}, \quad Y=\frac{(x-y)}{2}. \tag{2.5}$$

Here X and Y correspond to the synchronous and asynchronous modes of the orbit, respectively. For example, for a synchronous orbit $X=x$ and $Y=0$, whereas for an asynchronous orbit $Y\neq 0$.

In order to study the stability of a synchronous orbit with period q, we consider an infinitesimal perturbation $(\delta X,\delta Y)$ to the orbit. Here δX and δY correspond to the synchronous-mode and asynchronous-mode perturbations, respectively. Linearizing the q-times iterated map T^q (expressed in terms of the new coordinates) at an orbit point, we obtain a linearized map,

$$\begin{pmatrix} \delta X_{t+q} \\ \delta Y_{t+q} \end{pmatrix} = J \begin{pmatrix} \delta X_t \\ \delta Y_t \end{pmatrix}, \tag{2.6}$$

where the Jacobian matrix J ($\equiv DT^q$) of T^q is given by the q product of the Jacobian matrix DT of T along the orbit:

$$\begin{aligned} J &= \prod_{t=0}^{q-1} DT(x_t,x_t) \\ &= \prod_{t=0}^{q-1} \begin{pmatrix} f'(x_t) & 0 \\ 0 & f'(x_t)-2G(x_t) \end{pmatrix}. \end{aligned} \tag{2.7}$$

Here the prime denotes a derivative with respect to x, and $G(x)=\partial g(x,y)/\partial y|_{y=x}$; hereafter, $G(x)$ will be referred to as the ''reduced coupling function'' of $g(x,y)$. Note that δX and δY become decoupled for the case of a synchronous orbit (i.e., J has a diagonalized form).

The eigenvalues of J, called the stability multipliers of the orbit, are then given by

$$\lambda_0=\prod_{t=0}^{q-1} f'(x_t), \quad \lambda_1=\prod_{t=0}^{q-1} [f'(x_t)-2G(x_t)]. \tag{2.8}$$

The two stability multipliers, λ_0 and λ_1, determine the stability of the synchronous orbit against the synchronous-mode and asynchronous-mode perturbations, respectively. Hereafter, they will be called the synchronous and asynchronous stability multipliers, respectively. Note also that the synchronous stability multiplier λ_0 is just the stability multiplier of the uncoupled 1D map, and the coupling affects only the asynchronous stability multiplier λ_1.

A synchronous orbit is stable when it is stable against both the synchronous-mode and asynchronous-mode perturbations, i.e., the moduli of both stability multipliers are less than unity ($|\lambda_i|<1$ for $i=0,1$). Hence the stable region of a synchronous orbit in the parameter plane is bounded by the synchronous and asynchronous bifurcation lines determined by the equations $\lambda_i=\pm 1$ for $i=0,1$, as will be seen in Sec. III. When the $\lambda_0=1$ (-1) line is crossed, the synchronous orbit loses its stability via synchronous saddle-node (period-doubling) bifurcation. On the other hand, when the $\lambda_1=1$ (-1) line is crossed, it becomes unstable via asynchronous pitchfork (period-doubling) bifurcation. Some brief explanations on the bifurcations are given below.

In the case of a synchronous saddle-node bifurcation, the synchronous orbit collides with an unstable synchronous orbit with the same period, and then they disappear, like the tangent bifurcation in the 1D maps. On the other hand, there are two types of supercritical and subcritical bifurcations for each case of the pitchfork and period-doubling bifurcations. In the supercritical case of the synchronous (asynchronous) pitchfork and period-doubling bifurcations, the synchronous orbit loses its stability, and gives rise to the birth of a pair of new stable synchronous (asynchronous) orbits with the same period and a new stable synchronous (asynchronous) period-

doubled orbit, respectively. However, in the subcritical case of the synchronous (asynchronous) pitchfork and period-doubling bifurcations, the synchronous orbit becomes unstable by absorbing a pair of unstable synchronous (asynchronous) orbits with the same period and an unstable synchronous (asynchronous) period-doubled orbit, respectively. (For more details on bifurcations on 2D dissipative maps, refer to [15].)

B. Renormalization analysis

We now consider the period p-tupling renormalization transformation $\mathcal{N}$, which is composed of the p-times iterating ($T^{(p)}$) and rescaling (B) operators:

$$\mathcal{N}(T) \equiv B T^{(p)} B^{-1}. \tag{2.9}$$

Here the rescaling operator B is

$$B = \begin{pmatrix} \alpha & 0 \\ 0 & \alpha \end{pmatrix}, \tag{2.10}$$

because we consider only synchronous orbits.

Applying the renormalization operator $\mathcal{N}$ to the coupled map (2.1) n times, we obtain the n-times renormalized map T_n of the form

$$T_n : \begin{cases} x_{t+1} = F_n(x_t, y_t) = f_n(x_t) + g_n(x_t, y_t) \\ y_{t+1} = F_n(y_t, x_t) = f_n(y_t) + g_n(y_t, x_t). \end{cases} \tag{2.11}$$

Here f_n and g_n are the uncoupled and coupling parts of the n-times renormalized function F_n, respectively. They satisfy the following recurrence equations:

$$f_{n+1}(x) = \alpha f_n^{(p)}\left(\frac{x}{\alpha}\right), \tag{2.12}$$

$$g_{n+1}(x,y) = \alpha F_n^{(p)}\left(\frac{x}{\alpha}, \frac{y}{\alpha}\right) - \alpha f_n^{(p)}\left(\frac{x}{\alpha}\right), \tag{2.13}$$

where

$$f_n^{(p)}(x) = f_n(f_n^{(p-1)}(x)), \tag{2.14}$$

$$F_n^{(p)}(x,y) = F_n(F_n^{(p-1)}(x,y), F_n^{(p-1)}(y,x)), \tag{2.15}$$

and the rescaling factor is chosen to preserve the normalization condition $f_{n+1}(0) = 1$, i.e.,

$$\alpha = \frac{1}{f_n^{(p-1)}(1)}. \tag{2.16}$$

The recurrence relations (2.12) and (2.13) define a renormalization operator $\mathcal{R}$ of transforming a pair of functions (f,g):

$$\begin{pmatrix} f_{n+1} \\ g_{n+1} \end{pmatrix} = \mathcal{R}\begin{pmatrix} f_n \\ g_n \end{pmatrix}. \tag{2.17}$$

A map T_c with the nonlinearity and coupling parameters set to their critical values is called a critical map:

$$T_c : \begin{cases} x_{t+1} = F_c(x_t, y_t) = f_c(x_t) + g_c(x_t, y_t) \\ y_{t+1} = F_c(y_t, x_t) = f_c(y_t) + g_c(y_t, x_t). \end{cases} \tag{2.18}$$

A critical map is attracted to a fixed map T^* under iterations of the renormalization transformation $\mathcal{N}$:

$$T^* : \begin{cases} x_{t+1} = F^*(x_t, y_t) = f^*(x_t) + g^*(x_t, y_t) \\ y_{t+1} = F^*(y_t, x_t) = f^*(y_t) + g^*(y_t, x_t). \end{cases} \tag{2.19}$$

Here (f^*, g^*) is a fixed point of the renormalization operator $\mathcal{R}$ with $\alpha = 1/f^{*(p-1)}(1)$:

$$\begin{pmatrix} f^* \\ g^* \end{pmatrix} = \mathcal{R}\begin{pmatrix} f^* \\ g^* \end{pmatrix}. \tag{2.20}$$

This fixed-point equation can be solved row by row consecutively. Note that $f^*(x)$ is just the fixed function in the 1D map case, which varies depending on p [5,6,8,9]. Only the equation for the coupling fixed function $g^*(x,y)$ is therefore left to be solved. One trivial solution is $g^*(x,y) = 0$. In this zero-coupling case, the fixed map (2.19) consists of two uncoupled 1D fixed maps, which is associated with the CB at the zero-coupling critical point.

However, it is not easy to directly find coupling fixed functions other than the zero-coupling fixed function $g^*(x,y) = 0$. We therefore introduce a tractable recurrence equation for a reduced coupling function $G(x) = \partial g(x,y)/\partial y|_{y=x}$. Differentiating the recurrence equation (2.13) for $g(x,y)$ with respect to y and setting $y = x$, we obtain a recurrence equation for $G(x)$ [16]:

$$\begin{aligned} G_{n+1}(x) &= F_{n,2}^{(p)}\left(\frac{x}{\alpha}\right) \\ &= F_{n,2}^{(p-1)}\left(\frac{x}{\alpha}\right)\left[f_n'\left(f_n^{(p-1)}\left(\frac{x}{\alpha}\right)\right) - 2G_n\left(f_n^{(p-1)}\left(\frac{x}{\alpha}\right)\right)\right] \\ &\quad + f_n^{(p-1)\prime}\left(\frac{x}{\alpha}\right) G_n\left(f_n^{(p-1)}\left(\frac{x}{\alpha}\right)\right), \end{aligned} \tag{2.21}$$

where $F_{n,2}^{(p)}(x) \equiv \partial F_n^{(p)}(x,y)/\partial y|_{y=x}$. Then Eqs. (2.12) and (2.21) define a ''reduced renormalization operator'' $\widetilde{\mathcal{R}}$ of transforming a pair of functions (f,G):

$$\begin{pmatrix} f_{n+1} \\ G_{n+1} \end{pmatrix} = \widetilde{\mathcal{R}}\begin{pmatrix} f_n \\ G_n \end{pmatrix}. \tag{2.22}$$

We look for fixed points (f^*, G^*) of $\widetilde{\mathcal{R}}$, which satisfy

$$\begin{pmatrix} f^* \\ G^* \end{pmatrix} = \widetilde{\mathcal{R}}\begin{pmatrix} f^* \\ G^* \end{pmatrix}. \tag{2.23}$$

Here f^* is just the 1D fixed function and G^* is the reduced coupling fixed function of g^*, i.e., $G^*(x) = \partial g^*(x,y)/\partial y|_{y=x}$.

For the general period p-tupling case, we have [17]

$$F_{n,2}^{(p)}\left(\frac{x}{\alpha}\right) = 0 \quad \text{for} \quad G_n(x) = 0, \tag{2.24a}$$

$$F_{n,2}^{(p)}\left(\frac{x}{\alpha}\right)=\frac{1}{2}f_n^{(p)'}\left(\frac{x}{\alpha}\right) \quad \text{for } G_n(x)=\frac{1}{2}f_n'(x), \tag{2.24b}$$

$$F_{n,2}^{(p)}\left(\frac{x}{\alpha}\right)=\frac{1}{2}\left[f_n^{(p)'}\left(\frac{x}{\alpha}\right)-1\right] \quad \text{for } G_n(x)=\frac{1}{2}[f_n'(x)-1], \tag{2.24c}$$

$$F_{n,2}^{(p)}\left(\frac{x}{\alpha}\right)=\begin{cases}\frac{1}{2}\left[f_n^{(p)'}\left(\frac{x}{\alpha}\right)-1\right] & \text{for even } p\\ \frac{1}{2}\left[f_n^{(p)'}\left(\frac{x}{\alpha}\right)+1\right] & \text{for odd } p\end{cases}$$

$$\text{for } G_n(x)=\frac{1}{2}[f_n'(x)+1], \tag{2.24d}$$

$$F_{n,2}^{(p)}\left(\frac{x}{\alpha}\right)=\begin{cases}0 & \text{for even } p\\ f_n^{(p)'}\left(\frac{x}{\alpha}\right) & \text{for odd } p\end{cases}$$

$$\text{for } G_n(x)=f_n'(x). \tag{2.24e}$$

Differentiating the 1D fixed-function equation for $f^*(x)$ with respect to x in the period p-tupling case, we also have

$$f^{*'}(x)=f^{*(p)'}\left(\frac{x}{\alpha}\right)=\prod_{i=0}^{p-1} f^{*'}\left(f^{*(i)}\left(\frac{x}{\alpha}\right)\right). \tag{2.25}$$

Using Eqs. (2.24) and (2.25), we obtain three (five) solutions for $G^*(x)$ in the case of even (odd) p:

$$G^*(x)=0 \quad \text{for all } p, \tag{2.26a}$$

$$G^*(x)=\frac{1}{2}f^{*'}(x) \quad \text{for all } p, \tag{2.26b}$$

$$G^*(x)=\frac{1}{2}[f^{*'}(x)-1] \quad \text{for all } p, \tag{2.26c}$$

$$G^*(x)=\frac{1}{2}[f^{*'}(x)+1] \quad \text{for odd } p, \tag{2.26d}$$

$$G^*(x)=f^{*'}(x) \quad \text{for odd } p. \tag{2.26e}$$

Thus we find three (five) kinds of fixed points (f^*,G^*) of $\tilde{\mathcal{R}}$ for the case of even (odd) p.

In the case of a critical map (2.18), the synchronous and asynchronous stability multipliers $\lambda_{0,n}$ and $\lambda_{1,n}$ of the synchronous orbits are given by [see Eq. (2.8)]

$$\lambda_{0,n}=\prod_{t=0}^{q-1} f_c'(x_t), \quad \lambda_{1,n}=\prod_{t=0}^{q-1}[f_c'(x_t)-2G_c(x_t)], \tag{2.27}$$

where $G_c(x)$ is the reduced coupling function of $g_c(x)$, i.e., $G_c(x)=\partial g_c/\partial y|_{y=x}$. As $n\to\infty$, they converge to their limit values λ_0^* and λ_1^*, called the critical synchronous and asynchronous stability multipliers, respectively:

$$\lambda_0^*=\lim_{n\to\infty}\lambda_{0,n}, \quad \lambda_1^*=\lim_{n\to\infty}\lambda_{1,n}. \tag{2.28}$$

Here λ_0^* is just the critical stability multiplier λ^* for the 1D case, and the coupling affects only λ_1^*. The values of λ_1^* depend on the fixed points, as shown below.

The invariance of a fixed map T^* under iterations of the period p-tupling renormalization transformation $\mathcal{N}$ implies that, if T^* has a periodic point (x,y) with period p^n, then $B^{-1}(x,y)$ is a periodic point of T^* with period p^{n+1}. Since rescaling leaves the stability multipliers unaffected, all synchronous orbits of period p^n $(n=0,1,2,\ldots)$ have the same stability multipliers, which are just the critical stability multipliers. Consequently, they have the values of the stability multipliers of the fixed point of the fixed map T^*:

$$\lambda_0^*=f^{*'}(\hat{x}), \quad \lambda_1^*=f^{*'}(\hat{x})-2G^*(\hat{x}), \tag{2.29}$$

where $\hat{x}$ is the fixed point of the 1D fixed function [i.e., $\hat{x}=f^*(\hat{x})$], and λ_0^* is just the critical stability multiplier λ^* of the uncoupled 1D map. Note that λ_1^* depends on the reduced coupling fixed function $G^*(x)$:

$$\lambda_1^*=\lambda^* \quad \text{for } G^*(x)=0, \tag{2.30a}$$

$$\lambda_1^*=0 \quad \text{for } G^*(x)=\frac{1}{2}f^{*'}(x), \tag{2.30b}$$

$$\lambda_1^*=1 \quad \text{for } G^*(x)=\frac{1}{2}[f^{*'}(x)-1], \tag{2.30c}$$

$$\lambda_1^*=-1 \quad \text{for } G^*(x)=\frac{1}{2}[f^{*'}(x)+1], \tag{2.30d}$$

$$\lambda_1^*=-\lambda^* \quad \text{for } G^*(x)=f^{*'}(x), \tag{2.30e}$$

where the cases (2.30a) – (2.30c) exist for all p, but the cases (2.30d) and (2.30e) exist only for odd p.

Consider a pair of functions $(f^*,\tilde{G})$. Here $\tilde{G}(x)$ is not necessarily a reduced coupling fixed function $G^*(x)$. When $f_n(x)=f^*(x)$ and $G_n(x)=\tilde{G}(x)$, the function $F_{n,2}^{(p)}(x/\alpha)$ of Eq. (2.21) will be denoted by $\tilde{F}_2^{(p)}(x/\alpha)$. We now examine the evolution of a pair of functions $(f^*+h,\tilde{G}+\Phi)$ close to $(f^*,\tilde{G})$ under the reduced renormalization operator $\tilde{\mathcal{R}}$. Linearizing $\tilde{\mathcal{R}}$ at $(f^*,\tilde{G})$, we obtain a linearized operator $\tilde{\mathcal{L}}$ of transforming a pair of infinitesimal perturbations (h,Φ):

$$\begin{pmatrix}h_{n+1}\\ \Phi_{n+1}\end{pmatrix}=\tilde{\mathcal{L}}\begin{pmatrix}h_n\\ \Phi_n\end{pmatrix}=\begin{pmatrix}\tilde{\mathcal{L}}_1 & 0\\ \tilde{\mathcal{L}}_3 & \tilde{\mathcal{L}}_2\end{pmatrix}\begin{pmatrix}h_n\\ \Phi_n\end{pmatrix}, \tag{2.31}$$

where

$$h_{n+1}(x)=[\tilde{\mathcal{L}}_1 h_n](x)=\alpha\delta f_n^{(p)}\left(\frac{x}{\alpha}\right)\equiv\alpha\left[f_n^{(p)}\left(\frac{x}{\alpha}\right)-f^{*(p)}\left(\frac{x}{\alpha}\right)\right]_{\text{linear}}$$
$$=\alpha f^{*\prime}\left(f^{*(p-1)}\left(\frac{x}{\alpha}\right)\right)\delta f_n^{(p-1)}\left(\frac{x}{\alpha}\right)+\alpha h_n\left(f^{*(p-1)}\left(\frac{x}{\alpha}\right)\right), \tag{2.32}$$

$$\Phi_{n+1}(x)=[\tilde{\mathcal{L}}_2\Phi_n](x)+[\tilde{\mathcal{L}}_3 h_n](x)=\delta F_{n,2}^{(p)}\left(\frac{x}{\alpha}\right)\equiv\left[F_{n,2}^{(p)}\left(\frac{x}{\alpha}\right)-\tilde{F}_2^{(p)}\left(\frac{x}{\alpha}\right)\right]_{\text{linear}}, \tag{2.33}$$

$$[\tilde{\mathcal{L}}_2\Phi_n](x)=\left[f^{*\prime}\left(f^{*(p-1)}\left(\frac{x}{\alpha}\right)\right)-2\tilde{G}\left(f^{*(p-1)}\left(\frac{x}{\alpha}\right)\right)\right]\delta F_{n,2}^{(p-1)}\left(\frac{x}{\alpha}\right)+\left[f^{*(p-1)\prime}\left(\frac{x}{\alpha}\right)-2\tilde{F}_2^{(p-1)}\left(\frac{x}{\alpha}\right)\right]\Phi_n\left(f^{*(p-1)}\left(\frac{x}{\alpha}\right)\right), \tag{2.34}$$

$$[\tilde{\mathcal{L}}_3 h_n](x)=\left[\tilde{F}_2^{(p-1)}\left(\frac{x}{\alpha}\right)f^{*\prime\prime}\left(f^{*(p-1)}\left(\frac{x}{\alpha}\right)\right)-2\tilde{F}_2^{(p-1)}\left(\frac{x}{\alpha}\right)\tilde{G}'\left(f^{*(p-1)}\left(\frac{x}{\alpha}\right)\right)+f^{*(p-1)\prime}\left(\frac{x}{\alpha}\right)\tilde{G}'\left(f^{*(p-1)}\left(\frac{x}{\alpha}\right)\right)\right]\delta f_n^{(p-1)\prime}\left(\frac{x}{\alpha}\right)$$
$$+\tilde{F}_2^{(p-1)}\left(\frac{x}{\alpha}\right)h_n'\left(f^{*(p-1)}\left(\frac{x}{\alpha}\right)\right)+\tilde{G}\left(f^{*(p-1)}\left(\frac{x}{\alpha}\right)\right)\delta f_n^{(p-1)\prime}\left(\frac{x}{\alpha}\right). \tag{2.35}$$

Here the variations $\delta f_n^{(p)}(x/\alpha)$ and $\delta F_{n,2}^{(p)}(x/\alpha)$ are introduced as the linear terms (denoted by $[f_n^{(p)}(x/\alpha)-f^{*(p)}(x/\alpha)]_{\text{linear}}$ and $[F_{n,2}^{(p)}(x/\alpha)-\tilde{F}_2^{(p)}(x/\alpha)]_{\text{linear}}$) in h and Φ of the deviations of $f_n^{(p)}(x/\alpha)$ and $F_{n,2}^{(p)}(x/\alpha)$ from $f^{*(p)}(x/\alpha)$ and $\tilde{F}_2^{(p)}(x/\alpha)$, respectively.

When $\tilde{G}(x)$ is a reduced fixed coupling function $G^*(x)$ of Eq. (2.26), the operator $\tilde{\mathcal{L}}$ of Eq. (2.31) becomes a linearized transformation of $\tilde{\mathcal{R}}$ at a fixed point (f^*,G^*). A pair of perturbations (h^*,Φ^*) is then called an eigenperturbation with eigenvalue ν, if it satisfies

$$\nu\begin{pmatrix}h^*\\ \Phi^*\end{pmatrix}=\tilde{\mathcal{L}}\begin{pmatrix}h^*\\ \Phi^*\end{pmatrix}. \tag{2.36}$$

The reducibility of $\tilde{\mathcal{L}}$ into a semiblock form implies that to determine the eigenvalues of $\tilde{\mathcal{L}}$ it is sufficient to work independently in each of $h(x)$ subspace and $\Phi(x)$ subspace. That is, one can find eigenvalues of $\tilde{\mathcal{L}}_1$ and $\tilde{\mathcal{L}}_2$ separately and then they give the whole spectrum of $\tilde{\mathcal{L}}$.

We first solve the eigenvalue equation for $\tilde{\mathcal{L}}_1$, i.e.,

$$\nu h^*(x)=[\tilde{\mathcal{L}}_1 h^*](x). \tag{2.37}$$

Note that this is just the eigenvalue equation for the 1D map case. It has been shown that there exists only one relevant eigenvalue δ, associated with scaling of the nonlinearity parameter, whose values vary depending on p [2,4–10]. However, note that although the eigenvalue δ of $\tilde{\mathcal{L}}_1$ is also an eigenvalue of $\tilde{\mathcal{L}}$, $(h^*,0)$ is not an eigenperturbation of $\tilde{\mathcal{L}}$ unless $\tilde{\mathcal{L}}_3$ is a null operator.

We next consider a perturbation of the form $(0,\Phi)$ having only the coupling part. In this case $(0,\Phi^*)$ can be an eigenperturbation of $\tilde{\mathcal{L}}$, only if $\Phi^*(x)$ satisfies

$$\nu\Phi^*(x)=[\tilde{\mathcal{L}}_2\Phi^*](x). \tag{2.38}$$

Eigenvalues associated with coupling perturbations are called CE's.

For the case of coupling perturbation $(0,\Phi)$ to $(f^*,\tilde{G})$, $\tilde{\mathcal{L}}_2$ of Eq. (2.34) becomes

$$[\tilde{\mathcal{L}}_2\Phi](x)=\delta F_2^{(p)}\left(\frac{x}{\alpha}\right)$$
$$=\left[f^{*\prime}\left(f^{*(p-1)}\left(\frac{x}{\alpha}\right)\right)-2\tilde{G}\left(f^{*(p-1)}\left(\frac{x}{\alpha}\right)\right)\right]\times\delta F_2^{(p-1)}\left(\frac{x}{\alpha}\right)+\left[f^{*(p-1)\prime}\left(\frac{x}{\alpha}\right)-2\tilde{F}_2^{(p-1)}\left(\frac{x}{\alpha}\right)\right]\times\Phi\left(f^{*(p-1)}\left(\frac{x}{\alpha}\right)\right). \tag{2.39}$$

For the general period p-tupling case, we have [17]

$$\delta F_2^{(p)}\left(\frac{x}{\alpha}\right)=\sum_{i=0}^{p-1}f^{*(i)\prime}\left(\frac{x}{\alpha}\right)\Phi\left(f^{*(i)}\left(\frac{x}{\alpha}\right)\right)f^{*(p-1-i)\prime}\left(f^{*(i+1)}\left(\frac{x}{\alpha}\right)\right)\quad\text{for }\tilde{G}(x)=0, \tag{2.40a}$$

$$\delta F_2^{(p)}\left(\frac{x}{\alpha}\right)=0\quad\text{for }\tilde{G}(x)=\frac{1}{2}f^{*\prime}(x), \tag{2.40b}$$

$$\delta F_2^{(p)}\left(\frac{x}{\alpha}\right)=\sum_{i=0}^{p-1}\Phi\left(f^{*(i)}\left(\frac{x}{\alpha}\right)\right)\quad\text{for}\quad\widetilde{G}(x)=\frac{1}{2}[f^{*\prime}(x)-1], \tag{2.40c}$$

$$\delta F_2^{(p)}\left(\frac{x}{\alpha}\right)=\begin{cases}-\sum_{i=0}^{p-1}\Phi\left(f^{*(i)}\left(\frac{x}{\alpha}\right)\right) & \text{for even } p\\ \sum_{i=0}^{p-1}\Phi\left(f^{*(i)}\left(\frac{x}{\alpha}\right)\right) & \text{for odd } p\end{cases}\quad\text{for}\quad\widetilde{G}(x)=\frac{1}{2}[f^{*\prime}(x)+1], \tag{2.40d}$$

$$\delta F_2^{(p)}\left(\frac{x}{\alpha}\right)=\begin{cases}-\sum_{i=0}^{p-1}f^{*(i)\prime}\left(\frac{x}{\alpha}\right)\Phi\left(f^{*(i)}\left(\frac{x}{\alpha}\right)\right)f^{*(p-1-i)\prime}\left(f^{*(i+1)}\left(\frac{x}{\alpha}\right)\right) & \text{for even } p\\ \sum_{i=0}^{p-1}f^{*(i)\prime}\left(\frac{x}{\alpha}\right)\Phi\left(f^{*(i)}\left(\frac{x}{\alpha}\right)\right)f^{*(p-1-i)\prime}\left(f^{*(i+1)}\left(\frac{x}{\alpha}\right)\right) & \text{for odd } p\end{cases}\quad\text{for}\quad\widetilde{G}(x)=f^{*\prime}(x). \tag{2.40e}$$

For the case of even p, only the first three $\widetilde{G}$'s in Eqs. (2.40a) – (2.40c) are the reduced coupling fixed functions G^*'s, while for the case of odd p, all $\widetilde{G}$'s in Eqs. (2.40a) – (2.40e) are the reduced coupling fixed functions G^*'s.

We now find CE's associated with coupling perturbations. For the zero-coupling case of $G^*(x)=0$, the CE equation (2.38) becomes

$$\begin{aligned}\nu\Phi^*(x)&=[\widetilde{\mathcal{L}}_2\Phi^*](x)=\delta F_2^{(p)}\left(\frac{x}{\alpha}\right)\\&=\sum_{i=0}^{p-1}f^{*(i)\prime}\left(\frac{x}{\alpha}\right)\Phi^*\left(f^{*(i)}\left(\frac{x}{\alpha}\right)\right)\\&\quad\times f^{*(p-1-i)\prime}\left(f^{*(i+1)}\left(\frac{x}{\alpha}\right)\right).\end{aligned} \tag{2.41}$$

Using the fact that $f^{*\prime}(0)=0$, it can be easily shown that when $x=0$, Eq. (2.41) becomes

$$\nu\Phi^*(0)=\left(\prod_{i=1}^{p-1}f^{*\prime}(f^{*(i)}(0))\right)\Phi^*(0). \tag{2.42}$$

Letting $x\to 0$ in Eq. (2.25), we also have

$$\prod_{i=1}^{p-1}f^{*\prime}(f^{*(i)}(0))=\lim_{x\to 0}\frac{f^{*\prime}(x)}{f^{*\prime}(x/\alpha)}=\alpha. \tag{2.43}$$

Then Eq. (2.42) reduces to

$$\nu\Phi^*(0)=\alpha\Phi^*(0). \tag{2.44}$$

There are two cases. For the case $\Phi^*(0)\neq 0$, we have the first CE,

$$\nu_1=\alpha. \tag{2.45}$$

The eigenfunction $\Phi_1^*(x)$ with CE ν_1 is of the form

$$\Phi_1^*(x)=1+a_1x+a_2x^2+\cdots, \tag{2.46}$$

where a_i's $(i=1,2,\ldots)$ are some constants. For the other case $\Phi^*(0)=0$, it is found that $f^{*\prime}(x)$ is an eigenfunction for the CE equation (2.41). When $\Phi^*(x)=f^{*\prime}(x)$, Eq. (2.41) becomes

$$\nu f^{*\prime}(x)=pf^{*(p)\prime}\left(\frac{x}{\alpha}\right)=pf^{*\prime}(x). \tag{2.47}$$

We therefore have the second relevant CE,

$$\nu_2=p, \tag{2.48}$$

with reduced coupling eigenfunction

$$\Phi_2^*(x)=f^{*\prime}(x). \tag{2.49}$$

Note that $\Phi_2^*(x)$ has no constant term, while $\Phi_1^*(x)$ has a constant term. Thus we find two relevant CE's, $\nu_1=\alpha$ and $\nu_2=p$, for the zero-coupling case.

The nth image Φ_n of a general reduced coupling perturbation Φ under the linear transformation $\widetilde{\mathcal{L}}_2$ has the form

$$\begin{aligned}\Phi_n(x)&=[\widetilde{\mathcal{L}}_2^n\Phi](x)\\&\sim\alpha_1\nu_1^n\Phi_1^*(x)+\alpha_2\nu_2^n\Phi_2^*(x)\quad\text{for large } n,\end{aligned} \tag{2.50}$$

because the irrelevant part of Φ_n becomes negligibly small for large n. Here α_1 and α_2 are relevant components.

A coupling is called linear or nonlinear according to its leading term. In the case of a linear coupling, in which the coupling perturbation $\varphi(x,y)$ has a leading linear term, its reduced coupling function $\Phi(x)$ has a leading constant term, and hence $\Phi(0)\neq 0$. However, for any other case of nonlinear coupling with a leading nonlinear term, its reduced coupling function has no constant term, and hence $\Phi(0)=0$. Note that the relevant component α_1 becomes zero for the nonlinear-coupling case, while it is nonzero for the linear-coupling case. Consequently, the CB associated with coupling perturbations is governed by two relevant CE's, $\nu_1=\alpha$ and $\nu_2=p$, for the linear-coupling case, but by only one CE, $\nu_2=p$, for the nonlinear-coupling case, which will be confirmed in Sec. III.

We now consider the cases of two (four) other reduced coupling fixed functions $G^*(x)$'s for even (odd) p [see Eq. (2.26)]. They are associated with CB at critical points other than the zero-coupling critical point, as will be seen in Sec. III. Since $\delta F_2^{(p)}(x/\alpha)=0$ for $G^*(x)=\frac{1}{2}f^{*\prime}(x)$, $\tilde{\mathcal{L}}_2$ becomes a null operator. Hence there exist no CE's, and the CB is essentially the same as that for the 1D case. When $G^*(x)=\frac{1}{2}[f^{*\prime}(x)-1]$, the CE equation (2.38) becomes

$$\nu\Phi^*(x)=[\tilde{\mathcal{L}}_2\Phi^*](x)=\delta F_2^{(p)}\left(\frac{x}{\alpha}\right)$$
$$=\sum_{i=0}^{p-1}\Phi^*\left(f^{*(i)}\left(\frac{x}{\alpha}\right)\right). \tag{2.51}$$

There exists a relevant CE,

$$\nu=p, \tag{2.52}$$

when $\Phi^*(x)$ is a nonzero constant function, i.e., $\Phi^*(x)=b$ (b is a nonzero constant). For odd p there are two additional reduced coupling fixed functions, $G^*(x)=\frac{1}{2}[f^{*\prime}(x)+1]$ and $G^*(x)=f^{*\prime}(x)$. The CE equation (2.38) for $G^*(x)=\frac{1}{2}[f^{*\prime}(x)+1]$ is just that of Eq. (2.51). Therefore it has the same CE, $\nu=p$, as that for the case $G^*(x)=\frac{1}{2}[f^{*\prime}(x)-1]$. However, the critical asynchronous stability multipliers λ_1^* for the two cases are different [see Eq. (2.30)]. When $G^*(x)=f^{*\prime}(x)$, the CE equation (2.38) is the same as that for the case $G^*(x)=0$. Hence it also has two relevant CE's, $\nu_1=\alpha$ and $\nu_2=p$. However, λ_1^* for this case is different from that for the case $G^*(x)=0$, as can be seen in Eq. (2.30). The results of relevant CE's, along with those of the critical asynchronous stability multipliers, are listed in Table I.

III. LINEAR AND NONLINEAR COUPLINGS

We choose $f(x)=1-Ax^2$ as the uncoupled 1D map and consider two kinds of couplings, linear and nonlinear couplings. As examples of the linear- and nonlinear-coupling cases, we study the linearly and dissipatively coupled maps, respectively, and confirm the renormalization results. The structure of the critical set (set of the critical points) varies depending on the kind of coupling. In the linearly coupled case, an infinite number of critical line segments, together with the zero-coupling critical point, constitute the critical set, whereas in the dissipative case, the critical set consists of only one critical line segment, one end of which is the zero-coupling critical point. The CB also depends on the position on the critical set. For even (odd) p, three (four) kinds of fixed points govern the CB for the linearly coupled case, while only two (three) kinds of fixed points govern the CB for the dissipative case.

A. Linearly coupled maps

We numerically study the CB of period p-tuplings in two linearly coupled 1D maps with the coupling function

$$g(x,y)=\frac{c}{2}(y-x), \tag{3.1}$$

where c is the coupling parameter. The critical scaling behavior depends on whether p is even or odd.

As an example of odd period p-tuplings, we take the period-tripling case ($p=3$) and study its CB. The stability diagrams of synchronous orbits with period $q=3^n$ ($n=0,1,2,3$) are shown in Figs. 1 and 2. As noted in Sec. II A, the stable region of each synchronous orbit of level n (period 3^n) in the parameter plane is bounded by the four synchronous and asynchronous bifurcation curves determined by the equations $\lambda_{i,n}=\pm 1$ for $i=0,1$. Since each synchronous orbit of level n is created by its own synchronous saddle-node bifurcation (which occurs for $\lambda_{0,n}=1$), a sequence of stability regions with increasing n is not connected, unlike the period-doubling case [13]. We now examine the treelike structure of stability regions. Figure 1 shows the stability regions of synchronous orbits of the lowest two levels (i.e., $n=0$ and 1). The synchronous orbit with period $q=1$ is stable in some quadrilateral-shape region containing the $c=0$ line segment. However, the stability region of the next level $n=1$ consists of three quadrilateral-shape areas. They can be regarded as ''daughter'' quadrilaterals of the ''mother'' quadrilateral of level 0. That is, it may be thought that they branch off from the mother quadrilateral.

We next consider the stability regions of higher levels in Fig. 2. The branchings occur from the central one containing the $c=0$ line segment and its nearest-neighboring one (i.e., the right one) among the three quadrilaterals of level 1 [see Figs. 2(a) and 2(b)], while there is no branching from the left one [see Fig. 2(c)]. This rule governs the treelike structure of the stability regions. That is, for each level n branchings occur only from two quadrilateral-shape areas, the central one containing the $c=0$ line segment and its nearest-neighboring one. However, an infinite number of successive branchings occur only for the case of the central quadrilateral including the $c=0$ line segment [see Fig. 2(a)]. For the case of the nearest-neighboring quadrilateral, branching occurs only once, and after that, successive quadrilaterals of higher levels pile up without any further branchings [e.g., see Fig. 2(b)]. For the cases of quadrilaterals other than the central and its nearest-neighboring ones, successive quadrilaterals of higher levels pile up without any branchings [e.g., see Fig. 2(c)].

A sequence of stability regions with increasing period is called a ''period-tripling route,'' like the period-doubling case [13]. There are two kinds of period-tripling route. The sequence of the quadrilateral-shape areas containing the $c=0$ line segment converges to the zero-coupling point $c=0$ on the $A=A_\infty^{(3)}$ line, where $A_\infty^{(3)}$ ($=1.786\,440\,255\,563\,639\,354\,534\,447\ldots$) is the accumulation point of the period-tripling sequence for the 1D case. It will be referred to as the Z_3 route. On the other hand, a sequence of quadrilaterals which piles up without successive branchings converges to a critical line. For example, the leftmost one is the line joining two points c_l ($=-3.590\,291\,636\,032\,974\,400\,442\ldots$) and c_r ($=-3.482\,633\,674\,606\,564\,177\,473\ldots$) on the $A=A_\infty^{(3)}$ line [see Fig. 2(c)]. This kind of route will be called

TABLE I. Reduced coupling fixed functions $G^*(x)$, relevant CE's ν, and the critical asynchronous stability multipliers λ_1^* in all the period p-tupling cases are shown for the case of two-coupled maps. In the second column, e (o) denotes the even (odd) period-p tuplings. The first three for $G^*(x)$ exist for all p, while the last two exist only for odd p. Note also that the case $G^*(x)=\frac{1}{2}f^{*\prime}(x)$ has no relevant CE's, and α and λ^* are the orbital scaling factor and the critical stability multiplier for the 1D case, respectively.

$G^*(x)$	p	ν	λ_1^*
0	e, o	α, p	λ^*
$\frac{1}{2}\ f^{*\prime}$	e, o	nonexistent	0
$\frac{1}{2}[f^{*\prime}(x)-1]$	e, o	p	1
$\frac{1}{2}[f^{*\prime}(x)+1]$	o	p	-1
$f^{*\prime}(x)$	o	α, p	$-\lambda^*$

an L_3 route. Note that there are infinitely many L_3 routes, while the Z_3 route converging to the zero-coupling critical point $(A_\infty,0)$ is unique. Hence an infinite number of critical line segments, together with the zero-coupling critical point, constitute the critical set.

We now study the critical scaling behavior on the critical set. First, consider the case of the Z_3 route ending at the zero-coupling critical point. The CB for this zero-coupling case is governed by the zero-coupling fixed map (2.19) with $g^*(x,y)=0$, which has two relevant CE's, $\nu_1=\alpha$ $(=-9.277\,341\ldots)$ and $\nu_2=3$ (see Table I) as follows.

We follow the synchronous orbits of period $q=3^n$ up to level $n=10$ in the Z_3 route, and obtain a self-similar sequence of parameters (A_n,c_n), at which each orbit of level n has some given stability multipliers (λ_0,λ_1) (e.g., $\lambda_0=-1$ and $\lambda_1=1$). Then the sequence $\{(A_n,c_n)\}$ converges geometrically to the zero-coupling critical point $(A_\infty^{(3)},0)$. In order to see the convergence of each of the two scalar sequences $\{A_n\}$ and $\{c_n\}$, define $\delta_n\equiv\Delta A_n/\Delta A_{n+1}$ and $\mu_n\equiv\Delta c_n/\Delta c_{n+1}$, where $\Delta A_n=A_n-A_{n-1}$ and $\Delta c_n=c_n-c_{n-1}$. Then they converge to their limit values δ and μ, respectively, as shown in Table II. Hence the two sequences $\{A_n\}$ and $\{c_n\}$ obey one-term scaling laws asymptotically:

$$\Delta A_n\sim\delta^{-n},\quad \Delta c_n\sim\mu^{-n}\quad \text{for large } n, \tag{3.2}$$

where $\delta=55.247\ldots$ and $\mu=-9.277\ldots$. Note that the nonlinearity-parameter scaling factor δ is just that for the 1D case, and the value of the coupling-parameter scaling factor μ is close to that of the first CE, ν_1 $(=\alpha)$.

In order to take into account the effect of the second relevant CE, ν_2 $(=3)$, on the scaling of the sequence $\{\Delta c_n\}$, we extend the simple one-term scaling law (3.2) to a two-term scaling law [18]:

$$\Delta c_n\sim C_1\mu_1^{-n}+C_2\mu_2^{-n}\quad \text{for large } n, \tag{3.3}$$

where $|\mu_2|>|\mu_1|$, and C_1 and C_2 are some constants. This is a kind of multiple-scaling law [19]. Equation (3.3) gives

$$\Delta c_n=s_1\Delta c_{n+1}-s_2\Delta c_{n+2}, \tag{3.4}$$

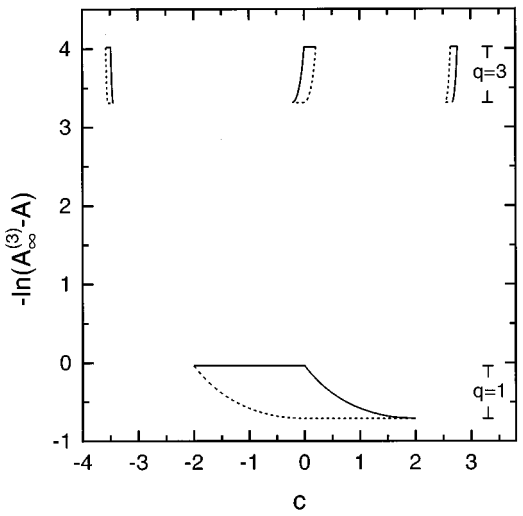

FIG. 1. Stability diagram of the synchronous 3^n-periodic orbits of the lowest two levels $n=0,1$ in two linearly coupled maps. Each periodic orbit of level n is born via its own saddle-node bifurcation. Its stable regions, denoted by $q=3^n$, are bounded by four bifurcation curves determined by $\lambda_i=\pm1$ for $i=0,1$. The horizontal and nonhorizontal solid (short-dashed) boundary lines [i.e., the $\lambda_0=-1$ (1) and $\lambda_1=-1$ (1) bifurcation curves] correspond to the synchronous and asynchronous period-doubling (synchronous saddle-node and asynchronous pitchfork) bifurcation curves, respectively.

where $s_1=\mu_1+\mu_2$ and $s_2=\mu_1\mu_2$. Then μ_1 and μ_2 are solutions of the following quadratic equation:

$$\mu^2-s_1\mu+s_2=0. \tag{3.5}$$

To evaluate μ_1 and μ_2, we first obtain s_1 and s_2 from Δc_n's using Eq. (3.4):

$$s_1=\frac{\Delta c_n\Delta c_{n+1}-\Delta c_{n-1}\Delta c_{n+2}}{\Delta c_{n+1}^2-\Delta c_n\Delta c_{n+2}},\quad s_2=\frac{\Delta c_n^2-\Delta c_{n+1}\Delta c_{n-1}}{\Delta c_{n+1}^2-\Delta c_n\Delta c_{n+2}}. \tag{3.6}$$

Note that Eqs. (3.3)–(3.6) hold only for large n. In fact the values of s_i's and μ_i's $(i=1,2)$ depend on the level n. Therefore we explicitly denote s_i's and μ_i's by $s_{i,n}$'s and $\mu_{i,n}$'s, respectively. Then each of them converges to a constant as $n\to\infty$:

$$\lim_{n\to\infty}s_{i,n}=s_i,\quad \lim_{n\to\infty}\mu_{i,n}=\mu_i,\quad i=1,2. \tag{3.7}$$

Three sequences $\{\mu_{1,n}\}$, $\{\mu_{2,n}\}$, and $\{\mu_{1,n}^2/\mu_{2,n}\}$ are shown in Table III. The second column shows rapid convergence of $\mu_{1,n}$ to its limit value μ_1 $(=-9.277341\ldots)$, which is close to the renormalization result of the first relevant CE, ν_1 $(=\alpha)$. (Its convergence to α is faster than that for the case of the above one-term scaling law.) From the third and fourth columns, we also find that the second scaling factor μ_2 is given by a product of two relevant CE's, ν_1 and ν_2,

$$\mu_2=\frac{\nu_1^2}{\nu_2}, \tag{3.8}$$

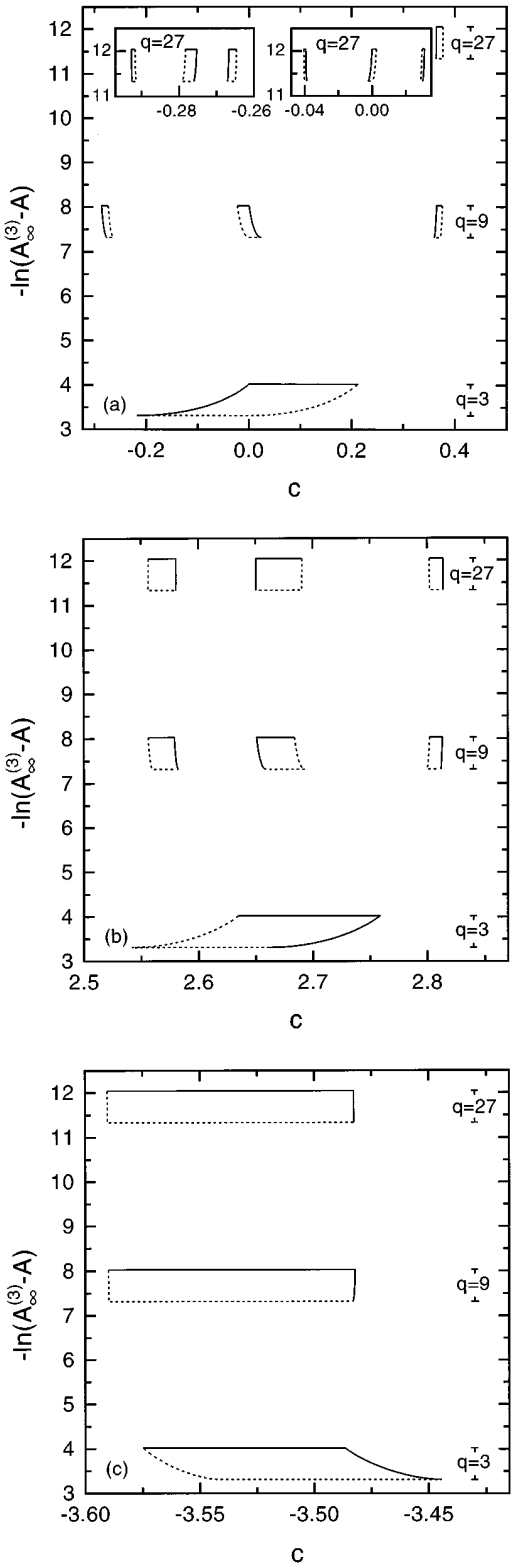

FIG. 2. Stability diagram of the synchronous 3^n-periodic ($n=1,2,3$) orbits of level n in two linearly coupled maps. Each periodic orbit of level n is created via its own saddle-node bifurcation. Its stable regions, denoted by $q=3^n$, are bounded by four bifurcation curves determined by $\lambda_i=\pm 1$ for $i=0,1$. The solid and short-dashed boundary lines represent the same as those in Fig. 1. The stability diagrams starting from the central, right, and left stability regions of level 1 are shown in (a), (b), and (c), respectively. See the text for other details.

where $\nu_1=\alpha$ and $\nu_2=3$. It has been known that every scaling factor in the multiple-scaling expansion of a parameter is expressed by a product of the eigenvalues of a linearized renormalization operator [19].

We also study the effect of CE's on the asynchronous stability multipliers of synchronous periodic orbits. Consider the two-coupled map (2.1) with $f(x)=f_c(x)$ and $g(x,y)=\varepsilon\varphi(x,y)$. Here $f_c(x)$ is the 1D critical map with the nonlinearity parameter set to its critical value $A=A_\infty^{(p)}$ and ε is an infinitesimal coupling parameter. The map for $\varepsilon=0$ is just the critical map T_c at the zero-coupling critical point consisting of two uncoupled 1D critical maps f_c. It is attracted to the zero-coupling fixed map (2.19) with $F^*(x,y)=f^*(x)$ under iterations of the renormalization transformation $\mathcal{N}$ of Eq. (2.9). Hence the reduced coupling function $G(x)$ $[=\varepsilon\Phi\equiv\varepsilon\partial\varphi(x,y)/\partial y|_{y=x}]$ corresponds to an infinitesimal reduced coupling perturbation to the reduced coupling fixed function $G^*(x)=0$.

In the period p-tupling case, the stability multipliers $\lambda_{0,n}$ and $\lambda_{1,n}$ of the p^n-periodic orbit are the same as those of the fixed point of the n times renormalized map $\mathcal{N}^n(T)$, which are given by

$$\lambda_{0,n}=f_n'(\hat{x}_n),$$

$$\lambda_{1,n}=f_n'(\hat{x}_n)-2G_n(\hat{x}_n)\simeq f_n'(\hat{x}_n)-2\varepsilon\Phi(\hat{x}_n). \quad (3.9)$$

Here (f_n,G_n) is the nth image of (f_c,G) under the reduced renormalization transformation $\tilde{\mathcal{R}}$, $\hat{x}_n$ is just the fixed point of $f_n(x)$ [i.e., $\hat{x}_n=f_n(\hat{x}_n)$] and converges to the fixed point $\hat{x}$ of the 1D fixed map $f^*(x)$ as $n\to\infty$. The first stability multiplier $\lambda_{0,n}$ converges to the 1D critical stability multiplier $\lambda^*=f^{*\prime}(\hat{x})$ as $n\to\infty$. For the period-tripling case, $\lambda^*=-1.872\,705\,929\ldots$. Since $G_n(x)\simeq[\tilde{\mathcal{L}}_2^nG](x)$ $=\varepsilon\Phi_n(x)$ [$\Phi_n(x)$ is given in Eq. (2.50)], the asynchronous stability multiplier has the form

$$\lambda_{1,n}\simeq\lambda_{0,n}-2\varepsilon\Phi_n(x)$$
$$\simeq\lambda^*+\varepsilon[e_1\nu_1^n+e_2\nu_2^n] \quad \text{for large } n, \quad (3.10)$$

where $e_1=-2\alpha_1\Phi_1^*(\hat{x})$ and $e_2=-2\alpha_2f^{*\prime}(\hat{x})$. Therefore the slope S_n of $\lambda_{1,n}$ at the zero-coupling critical point $(\varepsilon=0)$ is

$$S_n\equiv\frac{\partial\lambda_{1,n}}{\partial\varepsilon}\Big|_{\varepsilon=0}\simeq e_1\nu_1^n+e_2\nu_2^n \quad \text{for large } n. \quad (3.11)$$

Here the coefficients e_1 and e_2 depend on the initial reduced function $\Phi(x)$, because α_n's are determined only by $\Phi(x)$. Note that the coefficient e_1 is zero for the nonlinear-coupling case, whereas it is nonzero for the linear-coupling case. Hence the growth of S_n for large n is governed by the two relevant CE's, $\nu_1=\alpha$ and $\nu_2=p$, for the linear-coupling case, but only by the second relevant CE, $\nu_2=p$, for the nonlinear-coupling case.

Figure 3 shows three plots of $\lambda_{1,n}(A_\infty^{(3)},c)$ versus c for $n=2$, 3, and 4. The slope S_n of $\lambda_{1,n}$ at the zero-coupling critical point increases with n, and obeys well the two-term scaling law,

TABLE II. In the Z_3 route, we followed a sequence of parameters (A_n, c_n) at which the pair of stability multipliers $(\lambda_{0,n}, \lambda_{1,n})$ of the orbit of period 3^n is $(-1,1)$. This sequence converges to the zero-coupling critical point $(A_\infty^{(3)}, 0)$ with the scaling factors shown in the second and third columns.

n	δ_n	μ_n
3	55.264 789 71	−9.272 61
4	55.245 771 51	−9.279 20
5	55.247 110 93	−9.276 71
6	55.247 020 84	−9.277 55
7	55.247 026 98	−9.277 27
8	55.247 026 56	−9.277 36
9	55.247 026 59	−9.277 33

$$S_n \sim d_1 r_1^n + d_2 r_2^n \quad \text{for large } n, \tag{3.12}$$

where d_1 and d_2 are some constants and $|r_1| > |r_2|$. This equation gives

$$S_{n+2} = t_1 S_{n+1} - t_2 S_n, \tag{3.13}$$

where $t_1 = r_1 + r_2$ and $t_2 = r_1 r_2$. As in the scaling for the coupling parameter, we first obtain t_1 and t_2 of level n from S_n's:

$$t_{1,n} = \frac{S_{n+1}S_n - S_{n+2}S_{n-1}}{S_n^2 - S_{n+1}S_{n-1}}, \quad t_{2,n} = \frac{S_{n+1}^2 - S_n S_{n+2}}{S_n^2 - S_{n+1}S_{n-1}}. \tag{3.14}$$

Then the scaling factors $r_{1,n}$ and $r_{2,n}$ of level n are given by the roots of the quadratic equation, $r_n^2 - t_{1,n} r_n + t_{2,n} = 0$. They are listed in Table IV and converge to constants r_1 $(=\nu_1)$ and r_2 $(=\nu_2)$ as $n \to \infty$, whose accuracies are higher than those of the coupling-parameter scaling factors.

We next consider the cases of L_3 routes, each of which converges to a critical line segment. In each L_3 route, there are two kinds of self-similar sequences of parameters (A_n, c_n), at which each orbit of level n has some given stability multipliers; the one converges to the left end point of the critical line segment and the other converges to the right end point. As an example, consider the leftmost L_3 route [see Fig. 2(c)], which converges to the critical line segment with two ends $(A_\infty^{(3)}, c_l)$ and $(A_\infty^{(3)}, c_r)$. We follow, in the leftmost L_3 route, two self-similar sequences of parameters, one converging to the left end and the other converging to the right end. In both cases, the sequence $\{A_n\}$ converges geometrically to its accumulation value $A_\infty^{(3)}$ as in the case of the Z_3 route,

$$\Delta A_n \sim \delta^{-n} \quad \text{for large } n, \tag{3.15}$$

where $\Delta A_n = A_n - A_{n-1}$ and $\delta = 55.247\ldots$. The sequences $\{c_n\}$ for both cases also obey the one-term scaling law,

$$\Delta c_n \sim \mu^{-n} \quad \text{for large } n, \tag{3.16}$$

where $\Delta c_n = c_n - c_{n-1}$. The convergence of the scaling factor μ_n of level n to its limit value μ $(=3)$ is shown in Table V. Note that the value of μ is different from that $(\mu = \alpha)$ at the zero-coupling critical point. Although the scaling factors of the coupling parameter at both ends are the same, the critical asynchronous stability multipliers λ_1^* of Eq. (2.28) at both ends have different values. The convergence of the sequence $\{\lambda_{1,n}\}$ to its limit value λ_1^* is also shown in Table V. At the left (right) end, $\lambda_1^* = 1\,(-1)$. Comparing the values of μ and λ_1^* with those of the CE ν and λ_1^* listed in Table I, we find that the CB near the left end is governed by the fixed point (f^*, G^*) of $\tilde{\mathcal{R}}$ with $G^*(x) = \frac{1}{2}[f^{*'}(x) - 1]$, whereas that near the right end is governed by the fixed point with $G^*(x) = \frac{1}{2}[f^{*'}(x) + 1]$.

TABLE III. For the case of the Z_3 route, scaling factors $\mu_{1,n}$ and $\mu_{2,n}$ in the two-term scaling for the coupling parameter are shown in the second and third columns, respectively. A product of them, $\mu_{1,n}^2/\mu_{2,n}$, is shown in the fourth column.

n	$\mu_{1,n}$	$\mu_{2,n}$	$\mu_{1,n}^2/\mu_{2,n}$
4	−9.277 396 06	24.578 89	3.501 79
5	−9.277 337 31	27.768 52	3.099 52
6	−9.277 341 36	28.502 38	3.019 72
7	−9.277 341 10	28.650 77	3.004 08
8	−9.277 341 12	28.681 53	3.000 85

Figure 4 shows the behavior of the asynchronous stability multiplier $\lambda_{1,n}(A_\infty^{(3)}, c)$ near the leftmost critical line segment. The slopes S_n of $\lambda_{1,n}$ at both ends obey well the one-term scaling law,

$$S_n \sim \nu^n \quad \text{for large } n, \tag{3.17}$$

where $\nu = 3$. For any fixed value of c inside the critical line segment, $\lambda_{1,n}$ converges to zero as $n \to \infty$. That is, all the interior points are critical points with $\lambda_1^* = 0$. Hence the CB inside the critical line segment becomes the same as that of the 1D map, which will be discussed in more detail below. This kind of 1D-like CB is governed by the fixed point with $G^*(x) = \frac{1}{2} f^{*'}(x)$, which has no relevant CE's (see Table I).

For the case of a synchronous orbit in two linearly coupled 1D maps, its two Lyapunov exponents are given by

$$\sigma_0(A) = \lim_{m \to \infty} \frac{1}{m} \sum_{t=0}^{m-1} \ln |f'(x_t)|, \tag{3.18}$$

$$\sigma_1(A, c) = \lim_{m \to \infty} \frac{1}{m} \sum_{t=0}^{m-1} \ln |f'(x_t) - c|. \tag{3.19}$$

Here σ_0 (σ_1) is the synchronous (asynchronous) Lyapunov exponent characterizing the mean exponential rate of divergence of nearby orbits along (across) the symmetry line $y = x$. Note that the synchronous Lyapunov exponent σ_0 is just that of the uncoupled 1D map and the coupling affects only the asynchronous Lyapunov exponent σ_1. In order to see the phase dynamics near the critical line segment in more detail, we fix the value of the nonlinearity parameter $A = A_\infty^{(3)}$ and obtain the asynchronous Lyapunov exponent σ_1 of the synchronous orbit by varying the coupling parameter c, which is shown in Fig. 5. (Note that the synchronous Lyapunov exponent σ_0 of the synchronous quasiperiodic or-

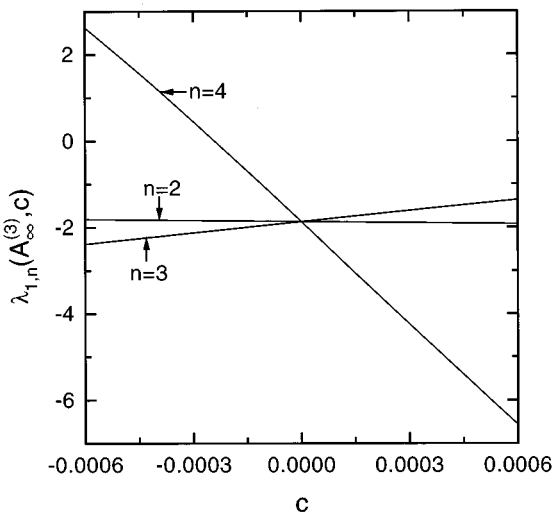

FIG. 3. Plots of the asynchronous stability multipliers $\lambda_{1,n}(A_\infty^{(3)},c)$ versus c near the zero-coupling critical point for the synchronous orbits of period $q=3^n$ $(n=2,3,4)$.

bit becomes zero on the $A=A_\infty^{(3)}$ line.) Inside the critical line segment $(c_l<c<c_r)$, the synchronous quasiperiodic orbit on the $y=x$ symmetry line becomes a synchronous attractor with $\sigma_1<0$. Since the dynamics on the synchronous attractor is the same as that for the uncoupled 1D case, the critical maps at interior points exhibit essentially 1D-like CB. However, as the coupling parameter c passes through c_l or c_r, the asynchronous Lyapunov exponent σ_1 of the synchronous quasiperiodic orbit increases from zero, and hence the coupling leads to desynchronization of the interacting systems. Thus the synchronous quasiperiodic orbit ceases to be an attractor outside the critical line segment, and new asynchronous attractors appear. This is illustrated in Fig. 6.

We also study the critical scaling behavior of the asynchronous Lyapunov exponent σ_1 near both ends for the case $A=A_\infty^{(3)}$. As shown in Fig. 7, the asynchronous Lyapunov exponent σ_1 varies linearly with respect to c near both ends, i.e., $\sigma_1\sim\varepsilon$, $\varepsilon\equiv c-c^*$ $(c^*=c_l$ or $c_r)$. The critical scaling behavior of σ_1 near both ends is obtained from the same CE, $\nu=3$, of the fixed points with $G^*(x)=\frac{1}{2}[1\pm f^{*'}(x)]$. Consider a map with nonzero ε (but with $A=A_\infty^{(3)}$) near both ends. It is then transformed into a new one of the same form, but with a renormalized parameter ε' under a renormalization transformation. Here the parameter ε obeys a scaling law,

$$\varepsilon'=\nu\varepsilon=3\varepsilon. \tag{3.20}$$

Then the asynchronous Lyapunov exponent σ_1 satisfies the homogeneity relation

$$\sigma_1(\varepsilon')=3\,\sigma_1(\varepsilon). \tag{3.21}$$

This leads to the scaling relation

$$\sigma_1(\varepsilon)\sim\varepsilon^{\eta}, \tag{3.22}$$

with exponent

$$\eta=\ln 3/\ln\nu=1. \tag{3.23}$$

TABLE IV. In the period-tripling case, scaling factors $r_{1,n}$ and $r_{2,n}$ in the two-term scaling for the slope S_n of the asynchronous stability multiplier $\lambda_{1,n}$ at the zero-coupling critical point are shown in the second and third columns, respectively.

n	$r_{1,n}$	$r_{2,n}$
4	−9.277 335 543 4	2.927 8
5	−9.277 341 501 0	2.984 5
6	−9.277 341 089 3	2.996 7
7	−9.277 341 117 4	2.999 3
8	−9.277 341 116 8	2.999 5

We now study the CB of period quadruplings $(p=4)$, as an example of even period-p tuplings. The stability diagrams of synchronous orbits of period $q=4^n$ $(n=0,1,2,3)$ are shown in Figs. 8 and 9. The treelike structure of stability regions is similar to that for the period-tripling case. As shown in Fig. 8, four ''daughter'' quadrilaterals of level 1 branch off from its ''mother'' quadrilateral of level 0. However, an infinite number of successive branchings occur only for the case of the central quadrilateral including the $c=0$ line [see Fig. 9(a)]. For the cases of quadrilaterals other than the central one, successive quadrilaterals of higher levels pile up without any branchings [see Figs. 9(b) and 9(c)].

Like the period-tripling case, there are two kinds of period-quadrupling route which are a sequence of stability regions with increasing period. The sequence of the quadrilaterals containing the $c=0$ line segment, called the Z_4 route, converges to the zero-coupling critical point $(A_\infty^{(4)},0)$, where $A_\infty^{(4)}$ $(=1.942\,704\,354\,755\,467\,972\,167\,178\ldots)$ is the accumulation point of the period-quadrupling sequence for the 1D case. On the other hand, a sequence of quadrilaterals which piles up without branchings, called an L_4 route, converges to a critical line. For example, the leftmost one is the line joining two points $(A_\infty^{(4)},c_l)$ and $(A_\infty^{(4)},c_r)$ [see Fig. 9(c)], where $c_l=-3.888\,058\,931\,772\,634\,488\ldots$ and $c_r=-3.877\,063\,178\,096\,222\,051\ldots$. Note also that there are infinitely many L_4 routes. Hence an infinite number of critical line segments, together with the zero-coupling critical point, constitute the critical set. The results of the critical scaling behavior on the critical set are given below.

We first consider the case of the Z_4 route ending at the zero-coupling critical point. As in the period-tripling case, the critical scaling behavior for this zero-coupling case is also governed by the zero-coupling fixed map with two relevant CE's, $\nu_1=\alpha$ $(=-38.819\,074\ldots)$ and $\nu_2=4$ as follows.

We follow, in the Z_4 route, the synchronous orbits of period $q=4^n$ up to level $n=7$, and obtain a self-similar sequence of parameters (A_n,c_n), at which the pair of stability multipliers $(\lambda_{0,n},\lambda_{1,n})$ of the 4^n-periodic orbit is $(-1,1)$. Then the sequence $\{(A_n,c_n)\}$ converges to the zero-coupling critical point $(A_\infty^{(4)},0)$. Here the sequence $\{A_n\}$ obeys well the one-term scaling law,

$$\Delta A_n\sim\delta^{-n} \quad \text{for large } n, \tag{3.24}$$

where $\Delta A_n=A_n-A_{n-1}$ and the scaling factor δ

TABLE V. We followed, in the leftmost L_3 route, two self-similar sequences of parameters. One sequence of parameters (A_n, c_n), at which $\lambda_{0,n}=-1$ and $\lambda_{1,n}=0.8$, converges to the left end $(A_\infty^{(3)}, c_l)$ of the critical line segment with the scaling factor μ_n of the coupling parameter shown in the second column. The other sequence of parameters (A_n, c_n), at which $\lambda_{0,n}=-1$ and $\lambda_{1,n}=-0.8$, converges to the right end $(A_\infty^{(3)}, c_r)$ with the scaling factor μ_n of the coupling parameter shown in the fourth column. In both cases the scaling factors are the same. The convergence of the sequence $\{\lambda_{1,n}\}$ to its limit values λ_1^* at the left (right) end is also shown in the third (fifth) column. Note that the values of λ_1^*'s at both ends are different.

n	μ_n	$\lambda_{1,n}$	μ_n	$\lambda_{1,n}$
3	3.664 5	0.996 763 57	1.836 2	−1.010 285 72
4	2.946 7	1.000 444 09	3.057 3	−0.998 599 423
5	2.990 8	0.999 939 19	2.968 2	−1.000 191 98
6	2.994 1	1.000 000 33	2.997 0	−0.999 973 71
7	2.998 3	0.999 998 86	2.998 0	−1.000 003 60
8	2.999 4	1.000 000 16	2.999 5	−0.999 999 51
9	2.999 8	0.999 999 98	2.999 8	−1.000 000 07

$(=981.594\ldots)$ is just the parameter scaling factor for the 1D case. On the other hand, the sequence $\{c_n\}$ obeys well the two-term scaling law,

$$\Delta c_n \sim C_1 \mu_1^n + C_2 \mu_2^n \quad \text{for large} \quad n, \tag{3.25}$$

where $\Delta c_n = c_n - c_{n-1}$, $|\mu_2| > |\mu_1|$, and C_1 and C_2 are some constants. As shown in Table VI, the two scaling factors μ_1 and μ_2 are given by

$$\mu_1 = \nu_1, \quad \mu_2 = \frac{\nu_1^2}{\nu_2}. \tag{3.26}$$

We also study the effect of the CE's on the asynchronous stability multipliers $\lambda_{1,n}$ of synchronous orbits. It is found

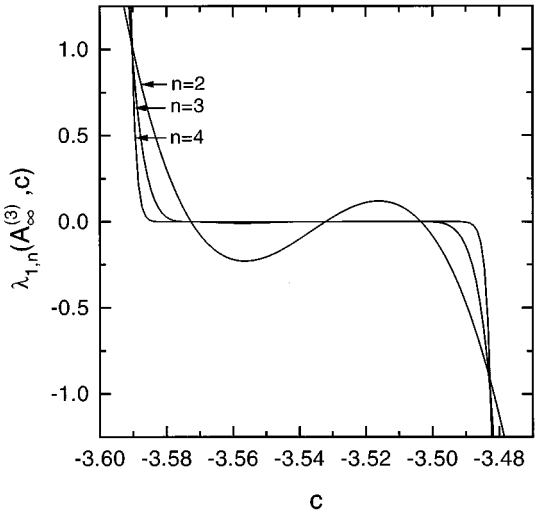

FIG. 4. Plots of the asynchronous stability multipliers $\lambda_{1,n}(A_\infty^{(3)}, c)$ versus c near the leftmost critical line for the synchronous orbits of period $q=3^n$ $(n=2,3,4)$.

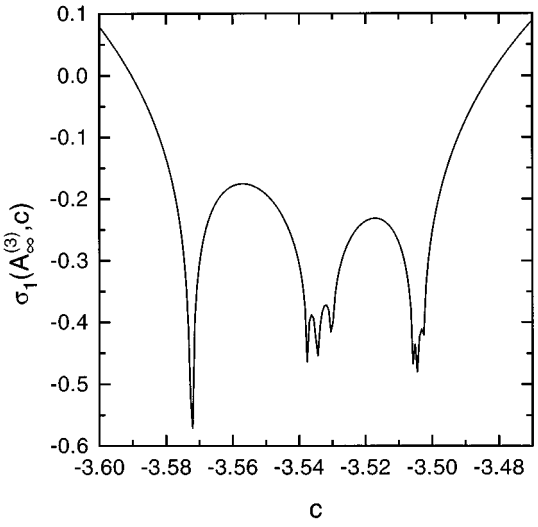

FIG. 5. Plot of the asynchronous Lyapunov exponent $\sigma_1(A_\infty^{(3)}, c)$ versus c near the leftmost critical line. The plot consists of 200 c values, each of which is obtained by iterating the map 100 000 times to eliminate transients and then averaging over another 500 000 iterations.

that the growth of the slope S_n of $\lambda_{1,n}$ at the zero-coupling critical point is also governed by the two CE's, i.e.,

$$S_n \sim d_1 \nu_1^n + d_2 \nu_2^n \quad \text{for large} \quad n, \tag{3.27}$$

where d_1 and d_2 are some constants.

We next consider the cases of L_4 routes, each of which ends at a critical line segment. As an example, consider the leftmost L_4 route [see Fig. 9(c)], in which we follow two self-similar sequences of parameters, one converging to the left end $(A_\infty^{(4)}, c_l)$ of the critical line segment and the other one converging to the right end $(A_\infty^{(4)}, c_r)$. As in the case of the Z_4 route, the sequence $\{A_n\}$ converges geometrically to its limit value $A_\infty^{(4)}$ with the 1D scaling factor δ. The sequence $\{c_n\}$ also obeys the one-term scaling law,

$$\Delta c_n \sim \mu^{-n} \quad \text{for large} \quad n, \tag{3.28}$$

where $\Delta c_n = c_n - c_{n-1}$. The convergence of the scaling factor μ_n of level n to its limit value μ is shown in Table VII. Note that the scaling factors μ at both ends are the same, i.e. $\mu=4$. Moreover, the critical asynchronous stability multipliers λ_1^* at both ends are also the same, i.e., $\lambda_1^*=1$, as shown in Table VII. This is in contrast to the period-tripling case where λ_1^*'s at both ends are different. We also compare the values of μ and λ_1^* with those of the CE ν and λ_1^* listed in Table I and find that the CB at both ends is governed by the same fixed point (f^*, G^*) of $\tilde{\mathcal{R}}$ with $G^*(x) = \frac{1}{2}[f^{*\prime}(x) - 1]$, unlike the period-tripling case.

Figure 10 shows the behavior of the asynchronous stability multiplier $\lambda_{1,n}(A_\infty^{(4)}, c)$ near the leftmost critical line segment. The growth of the slope S_n of $\lambda_{1,n}$ at both ends is governed by the CE ν $(=4)$, i.e.,

$$S_n \sim \nu^n \quad \text{for large} \quad n. \tag{3.29}$$

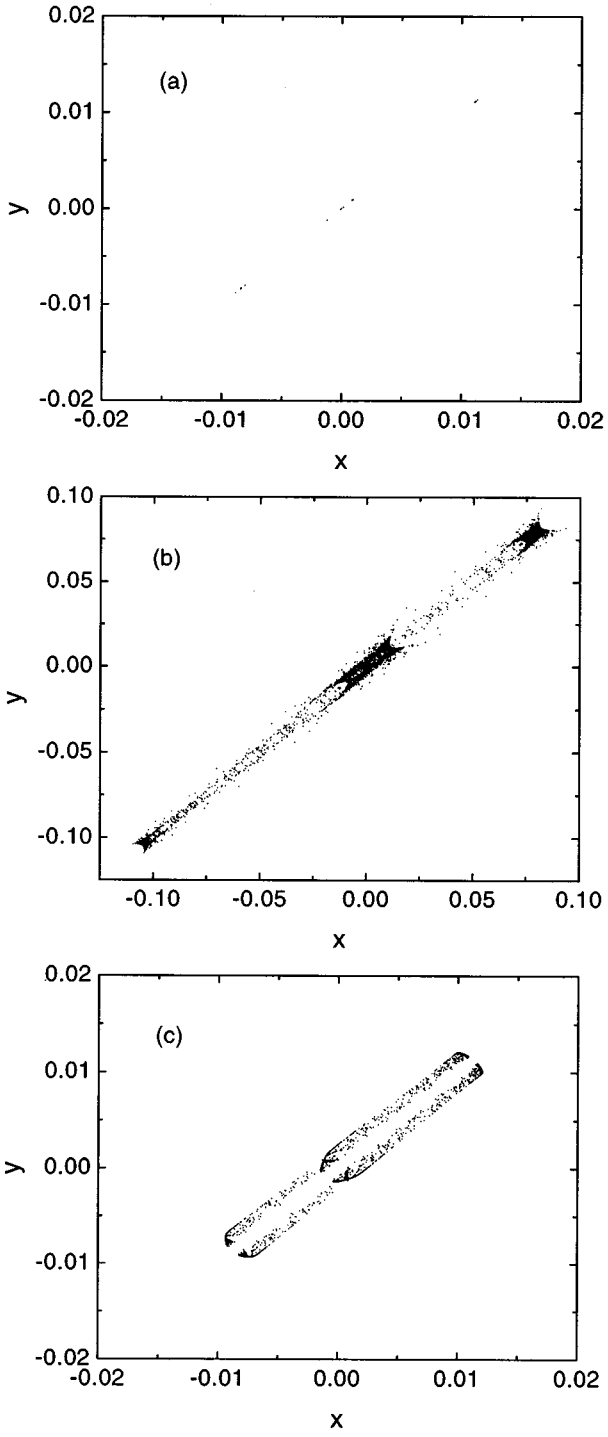

FIG. 6. Attractors near the leftmost critical line: (a) a synchronous attractor inside the critical line and asynchronous attractors outside the critical line for (b) $c=-3.590\,5$ and (c) $c=-3.482\,4$. For each case, the map is iterated 100 000 times to eliminate transients and the next 10 000 iterations are plotted.

However, for any fixed value of c inside the critical line segment, $\lambda_{1,n}$ converges to zero as $n\to\infty$. Thus all the interior points become critical ones with $\lambda_1^*=0$. Consequently, the CB inside the critical line segment becomes the same as that of the 1D map, as will be seen below. This kind of 1D-like CB is governed by the fixed point with $G^*(x)=\frac{1}{2}f^{*\prime}(x)$, which has no relevant CE's (see Table I).

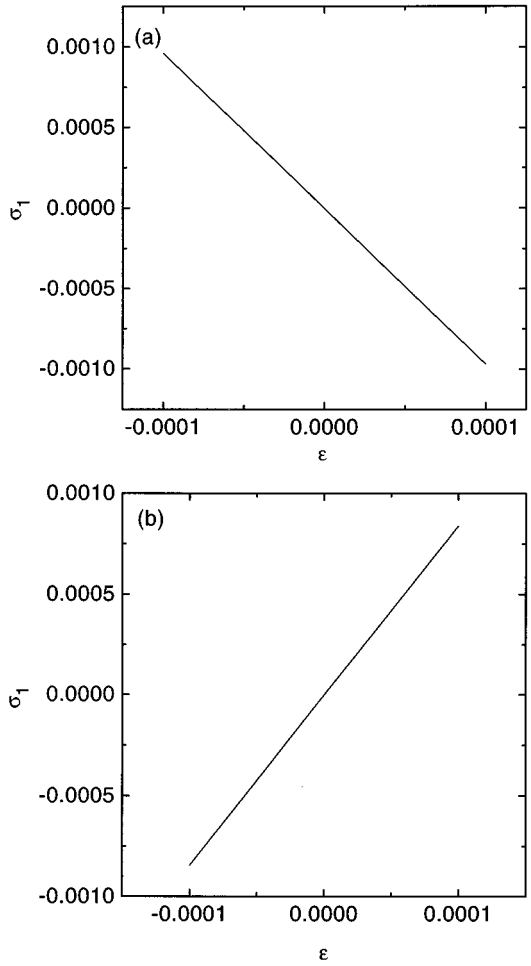

FIG. 7. Plots of the asynchronous Lyapunov exponent $\sigma_1(A_\infty^{(3)},\varepsilon)$ versus ε ($\varepsilon\equiv c-c^*, c^*=c_l$ or c_r) near the (a) left and (b) right ends of the leftmost critical line. Each plot consists of 50 ε values, each of which is obtained by iterating the map 100 000 times to eliminate transients and then averaging over another 500 000 iterations.

In order to see the phase dynamics near the critical line segment in more detail, we fix the value of the nonlinearity parameter $A=A_\infty^{(4)}$ and obtain the asynchronous Lyapunov exponent σ_1 [see Eq. (3.19)] of the synchronous orbit by varying the coupling parameter c, which is shown in Fig. 11. Inside the critical line segment ($c_l<c<c_r$), the synchronous quasiperiodic orbit on the $y=x$ symmetry line becomes a synchronous attractor with $\sigma_1<0$, as shown in Fig. 12(a). Note that the dynamics on the synchronous attractor is the same as that for the uncoupled 1D case. Hence the critical maps inside the critical line segment exhibit 1D-like CB. However, as the coupling parameter c passes through c_l or c_r, the asynchronous Lyapunov exponent σ_1 of the synchronous quasiperiodic orbit increases from zero, and hence the coupling leads to desynchronization of the interacting systems. Thus the synchronous quasiperiodic orbit ceases to be an attractor outside the critical line segment, and new asynchronous attractors appear, as shown in Figs. 12(b) and 12(c).

We also study the scaling behavior of the asynchronous Lyapunov exponent σ_1 near both ends of the critical line

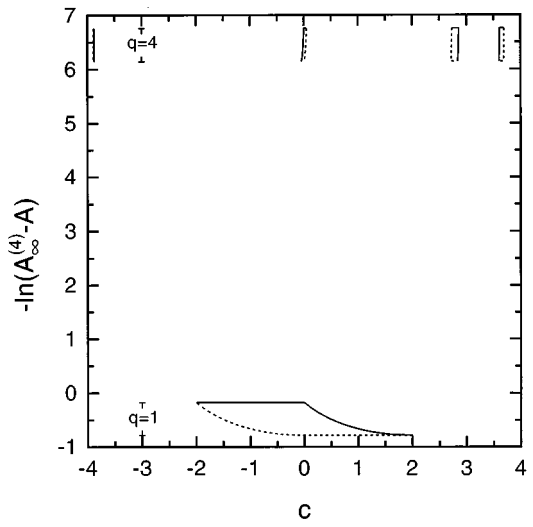

FIG. 8. Stability diagram of the synchronous 4^n-periodic orbits of the lowest two levels $n=0,1$ in two linearly coupled maps. Each periodic orbit of level n is created via its own saddle-node bifurcation. Its stable regions, denoted by $q=4^n$, are bounded by four bifurcation curves determined by $\lambda_i=\pm 1$ for $i=0,1$. The solid and short-dashed boundary lines represent the same as those in Fig. 1.

segment. As in the period-tripling case, using the scaling theory, one can also obtain the scaling relation of σ_1, $\sigma_1 \sim \epsilon^\eta$ with exponent $\eta=\ln 4/\ln\nu=1$, where ν $(=4)$ is the CE of the fixed point with $G^*(x)=\frac{1}{2}[f^{*'}(x)-1]$. Hence the asynchronous Lyapunov exponent σ_1 varies linearly with respect to c near both ends.

Finally, we briefly summarize the results for the linear-coupling case. The critical set consists of the zero-coupling critical point and an infinite number of critical line segments. The CB at the zero-coupling critical point is governed by the zero-coupling fixed map with two CE's, ν_1 $(=\alpha)$ and ν_2 $(=p)$, for all period p-tupling cases. However, the CB near both ends of each critical line segment depends on whether p is even or odd. In the case of odd p, the CB at one end is governed by a fixed point (f^*,G^*) of $\tilde{\mathcal{R}}$ with $G^*(x)=\frac{1}{2}[1-f^{*'}(x)]$ and that at the other end by another fixed point with $G^*(x)=\frac{1}{2}[1+f^{*'}(x)]$. These two fixed points have only one CE, $\nu=p$. On the other hand, in the case of even p, the CB at both ends is governed by the same fixed point with $G^*(x)=\frac{1}{2}[f^{*'}(x)-1]$. Inside the critical line segment, the CB is the same as that of the 1D map for all period p-tupling cases. This kind of 1D-like CB is governed by the fixed point with $G^*(x)=\frac{1}{2}f^{*'}(x)$, which has no relevant CE's. Consequently, for even (odd) p, three (four) kinds of fixed points govern the CB for the linearly coupled case.

B. Dissipatively coupled maps

As an example of the nonlinear-coupling case, we consider two dissipatively coupled 1D maps with the coupling function

$$g(x,y)=\frac{c}{2}[f(y)-f(x)], \tag{3.30}$$

and study the CB of the period triplings $(p=3)$ and period quadruplings $(p=4)$.

Figures 13(a) and 13(b) show the stability diagrams of synchronous orbits with period $q=p^n$ $(n=1,2,3)$ for $p=3$ and 4, respectively. As previously shown, each stability region of level n (period p^n) in the parameter plane is bounded by four bifurcation curves determined by $\lambda_{i,n}=\pm 1$ for $i=0,1$. An infinite sequence of such stability regions, called the ''period p-tupling route,'' converges to a critical line joining two ends $(A_\infty^{(p)},c_l^*)$ and $(A_\infty^{(p)},c_r^*)$, where $A_\infty^{(p)}$ is the accumulation point of the period p-tupling sequence for the 1D case, $c_l^*=0$ and $c_r^*=2$, as shown below. Hence only one critical line segment constitutes the critical set for the dissipative case, unlike the linearly coupled case.

Consider two dissipatively coupled 1D maps on the line $A=A_\infty^{(p)}$ in the parameter plane, in which case the reduced coupling function of the coupling function (3.30) is given by

$$G(x)=\frac{c}{2}f_c'(x), \tag{3.31}$$

where f_c is the 1D critical map with the nonlinearity parameter set to its critical value. By successive applications of the renormalization operator $\tilde{\mathcal{R}}$ to (f_c,G), we have

$$f_n(x)=\alpha f_{n-1}^{(p)}\left(\frac{x}{\alpha}\right), \quad G_n(x)=\frac{c_n}{2}f_n'(x), \tag{3.32}$$

$$c_n=c_{n-1}^3-3c_{n-1}^2+3c_{n-1} \quad \text{for } p=3, \tag{3.33}$$

$$c_n=-c_{n-1}^4+4c_{n-1}^3-6c_{n-1}^2+4c_{n-1} \quad \text{for } p=4, \tag{3.34}$$

where $f_0(x)=f_c(x)$, $G_0(x)=G(x)$, and $c_0=c$. Here f_n converges to the 1D fixed map $f^*(x)$.

The fixed points of the recurrence equations (3.33) and (3.34) for c are denoted by solid circles in Fig. 14. For $p=3$, there are three fixed points,

$$c^*=0,\ 1,\ 2, \tag{3.35}$$

while only two fixed points,

$$c^*=0,\ 1, \tag{3.36}$$

exist for $p=4$. Stability of a fixed point c^* is determined by its stability multiplier λ given by $\lambda=dc_n/dc_{n-1}|_{c^*}$. Note that the fixed point at $c^*=1$ is superstable $(\lambda=0)$. The basin of attraction to the superstable fixed point becomes the open interval (0,2), because any initial c inside the interval $0<c<2$ converges to $c^*=1$. For the period-tripling case, both ends $c_l^*=0$ and $c_r^*=2$ of the interval are unstable fixed points with $\lambda=3$, and all points outside the interval diverge to the plus or minus infinity. However, for the quadrupling case, only the left end $c_l^*=0$, which is also the image of the right end $c_r^*=2$ under the recurrence relation (3.34), is an unstable fixed point with $\lambda=4$, and all points outside the interval diverge to the minus infinity. Thus the line segment connecting two end points $c_l^*=0$ and $c_r^*=2$ becomes the critical line for the dissipative-coupling case.

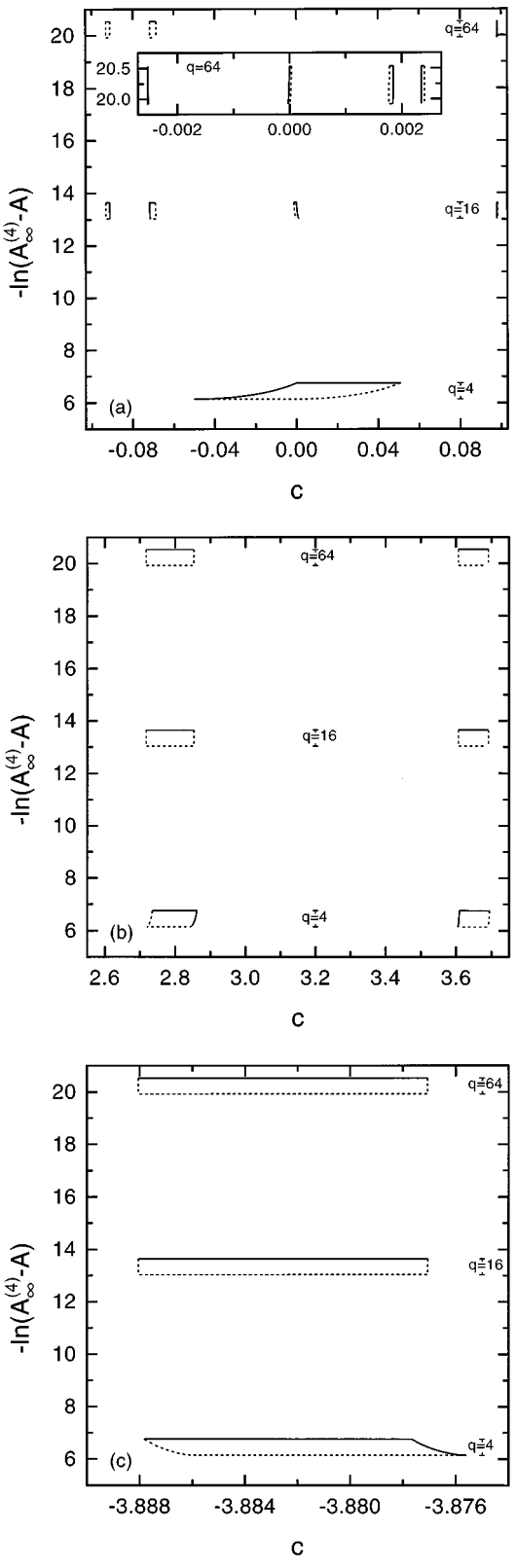

FIG. 9. Stability diagram of the synchronous 4^n-periodic orbits of level n ($n=1,2,3$) in two linearly coupled maps. Each periodic orbit of level n is created via its own saddle-node bifurcation. Its stable regions, denoted by $q=4^n$, are bounded by four bifurcation curves determined by $\lambda_i=\pm 1$ for $i=0,1$. The solid and short-dashed boundary lines represent the same as those in Fig. 1. The stability diagrams starting from the central, right, and left stability regions of level 1 are shown in (a), (b), and (c), respectively. See the text for other details.

TABLE VI. For the case of the Z_4 route, scaling factors $\mu_{1,n}$ and $\mu_{2,n}$ in the two-term scaling for the coupling parameter are shown in the second and third columns, respectively. A product of them, $\mu_{1,n}^2/\mu_{2,n}$, is shown in the fourth column.

n	$\mu_{1,n}$	$\mu_{2,n}$	$\mu_{1,n}^2/\mu_{2,n}$
3	−38.819 021 99	311.92	4.83
4	−38.819 074 56	372.98	4.04
5	−38.819 074 24	377.22	3.99

All critical maps inside the critical line segment are attracted to the fixed maps with the same reduced coupling function $G^*(x)=\frac{1}{2}f^{*'}(x)$. These fixed maps have no relevant CE's, because the fixed point $c^*=1$ is superstable. Hence the critical maps at interior points exhibit essentially 1D-like CB. In the period-tripling case, the critical map at the left end c_l^* is attracted to the zero-coupling fixed map,

$$T^*: x_{t+1}=f^*(x_t), \quad y_{t+1}=f^*(y_t), \tag{3.37}$$

with the reduced coupling function $G^*(x)=0$, and the critical map at the right end c_r^* to another fixed map,

$$T^*: x_{t+1}=f^*(y_t), \quad y_{t+1}=f^*(x_t), \tag{3.38}$$

with the reduced coupling fixed function $G^*(x)=f^{*'}(x)$. However, in the period-quadrupling case, the critical maps at both ends are attracted to the zero-coupling fixed map (3.37). Note that the two fixed maps of Eqs. (3.37) and (3.38) have the same relevant CE's, $\nu_1=\alpha$ and $\nu_2=p$ (see Table I). However, for this dissipatively coupled case, the CB's near both ends are governed only by the second CE, $\nu_2=p$ [i.e., the first relevant component α_1 in Eq. (2.50) becomes zero], which can be easily understood from the fact that the fixed points $c^*=0,2$ are unstable ones with stability multiplier $\lambda=p$.

We study the critical scaling behavior associated with coupling near the critical line segment and confirm the renor-

TABLE VII. We followed, in the leftmost L_4 route, two self-similar sequences of parameters (A_n,c_n), at which $\lambda_{0,n}=-1$ and $\lambda_{1,n}=0.8$. One sequence converges to the left end $(A_\infty^{(4)},c_l)$ of the critical line segment with the scaling factor μ_n of the coupling parameter shown in the second column. The other sequence converges to the right end $(A_\infty^{(4)},c_r)$ with the scaling factor μ_n of the coupling parameter shown in the fourth column. In both cases the scaling factors are the same. The convergence of the sequence $\{\lambda_{1,n}\}$ to its limit values λ_1^* at the left (right) end is also shown in the third (fifth) column. Note that the values of λ_1^*'s at both ends are the same.

n	μ_n	$\lambda_{1,n}$	μ_n	$\lambda_{1,n}$
2	5.013	1.010 032 65	50.70	0.987 196 90
3	4.051	0.999 630 89	3.674	1.000 476 66
4	3.963	1.000 013 65	3.978	0.999 982 38
5	3.992	0.999 999 50	3.993	1.000 000 65
6	3.998	1.000 000 02	3.998	0.999 999 98

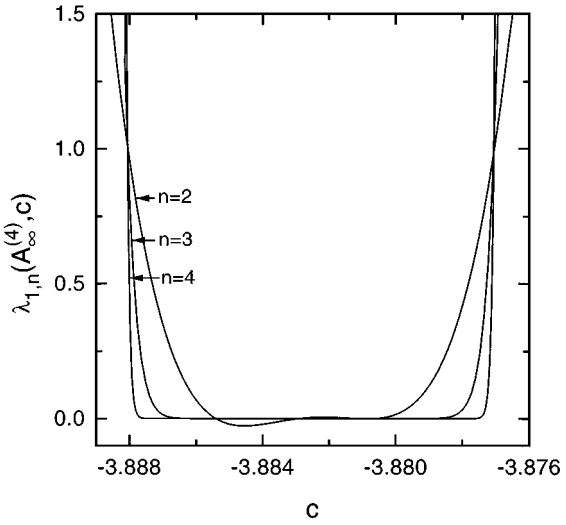

FIG. 10. Plots of the asynchronous stability multipliers $\lambda_{1,n}(A_\infty^{(4)},c)$ versus c near the leftmost critical line for the synchronous orbits of period 4^n $(n=2,3,4)$.

malization results. For the dissipative-coupling case, the stability multipliers of synchronous orbits with period $q=p^n$ $(p=3,4)$ become

$$\lambda_{0,n}(A)=\prod_{t=0}^{q-1} f'(x_t), \quad \lambda_{1,n}(A,c)=(1-c)^q\lambda_{0,n}. \tag{3.39}$$

Let the pair of stability multipliers of the synchronous orbit of level n (period p^n) at a point (A,c) be (λ_0,λ_1). Then there exists a ''conjugate point'' $(A,-c+2)$, at which the pair of stability multipliers becomes $(\lambda_0,-\lambda_1)$ and (λ_0,λ_1) for $p=3$ and 4, respectively. For $c=1$, $\lambda_1=0$ and the two conjugate points become degenerate.

Like the linearly coupled case, we follow the synchronous orbits of level n in the period p-tupling route, and obtain a

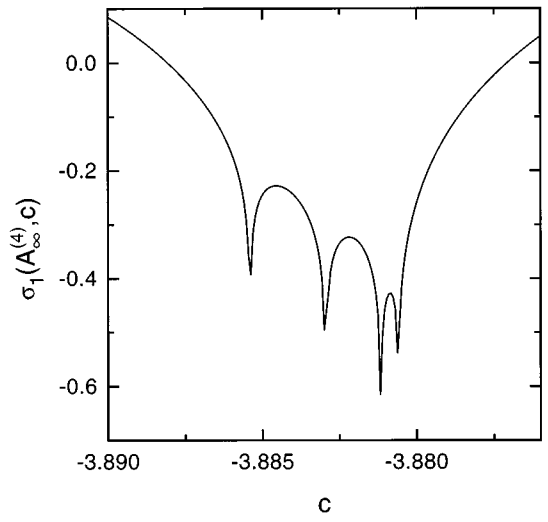

FIG. 11. Plot of the asynchronous Lyapunov exponent $\sigma_1(A_\infty^{(4)},c)$ versus c near the leftmost critical line. The plot consists of 200 c values, each of which is obtained by iterating the map 100 000 times to eliminate transients and then averaging over another 500 000 iterations.

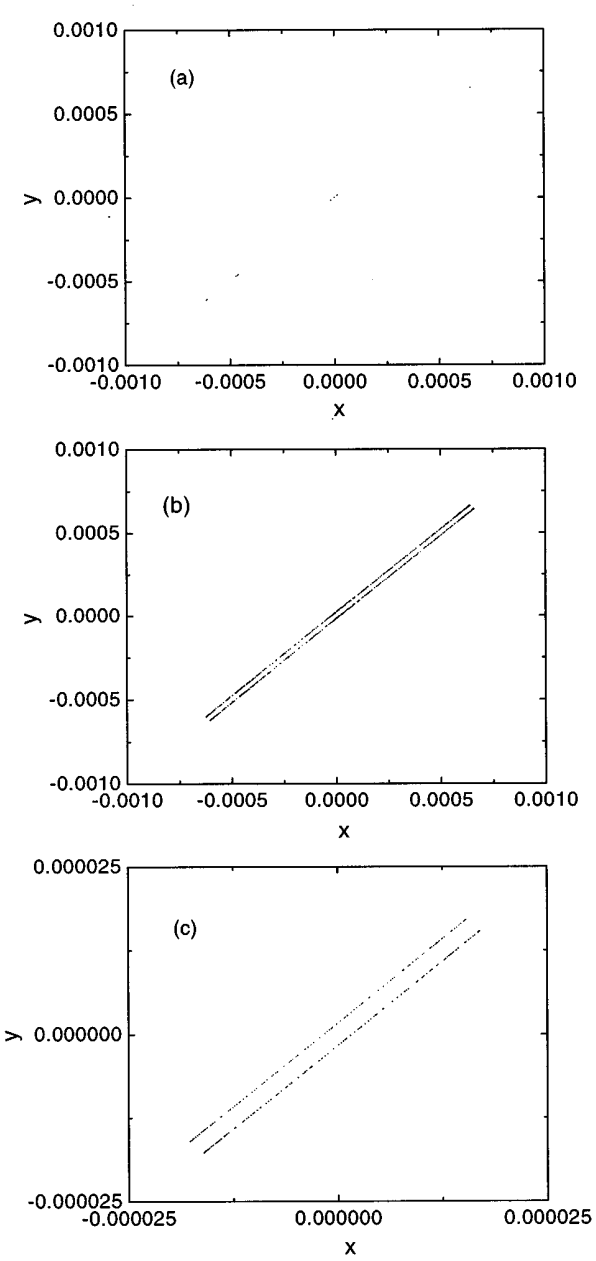

FIG. 12. Attractors near the leftmost critical line: (a) a synchronous attractor inside the critical line and asynchronous attractors outside the critical line for (b) $c=-3.877\,059$ and (c) $c=-3.888\,059$. For each case, the map is iterated 100 000 times to eliminate transients and the next 10 000 iterations are plotted.

self-similar sequence of parameters (A_n,c_n), at which each orbit of level n has some given stability multipliers (λ_0,λ_1). Without loss of generality, we choose $\lambda_0=-1$. Then one can find a pair of mutually conjugate sequences. One sequence $\{(A_n,c_n)\}$ can be obtained by fixing $-1<\lambda_1<0$, which converges to the zero-coupling critical point $(A_\infty^{(p)},0)$ as follows:

$$A_n-A_\infty^{(p)}\sim\delta^{-n}, \quad c_n=1-(-\lambda_1)^{p^{-n}}\sim-\ln(-\lambda_1)p^{-n} \quad \text{for large } n, \tag{3.40}$$

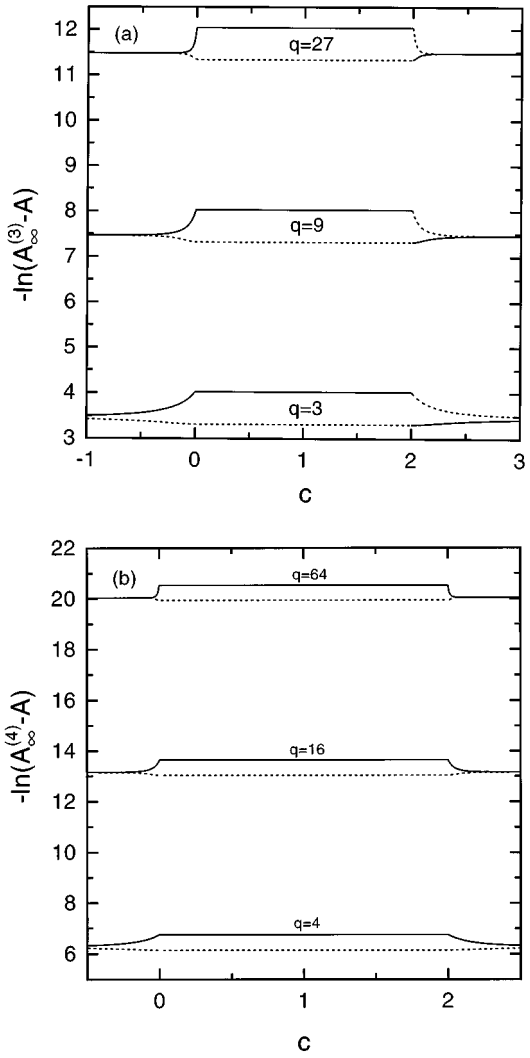

FIG. 13. Stability diagram of the synchronous orbits for the (a) period-tripling ($p=3$) and (b) period-quadrupling ($p=4$) cases in two dissipatively coupled maps. Each periodic orbit of level n is born via its own saddle-node bifurcation. Its stable regions, denoted by $q=p^n$ ($n=1,2,3$), are bounded by four bifurcation curves determined by $\lambda_i=\pm 1$ for $i=0,1$. The solid and short-dashed boundary lines represent the same as those in Fig. 1.

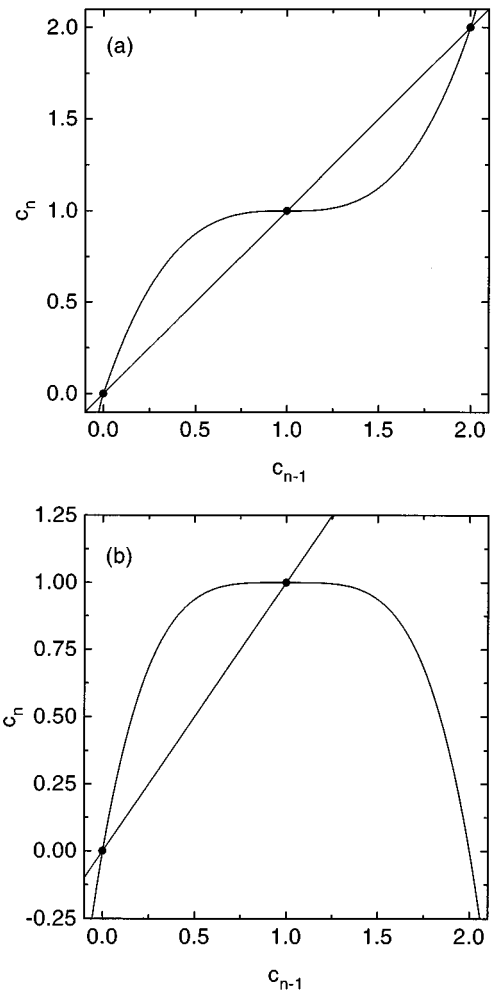

FIG. 14. Fixed points of the recurrence equations (a) (3.33) and (b) (3.34). The intersection points between the curves of Eqs. (3.33) and (3.34) and the line $c_n=c_{n-1}$ are just the fixed points, denoted by solid circles.

where $A_\infty^{(p)}$ and δ are just those for the 1D case. Note that the coupling-parameter scaling factor is just the second relevant CE, ν_2 $(=p)$, of the zero-coupling fixed map (3.37). The ''conjugate sequence'' can also be obtained by following p^n-periodic orbits with $\lambda_{1,n}=-\lambda_1$ and λ_1 for $p=3$ and 4, respectively. This kind of conjugate sequence $\{(A_n,c_n)\}$ converges to the right-end critical point $(A_\infty^{(p)},2)$ (i.e., the conjugate point of the zero-coupling critical point) as follows:

$$A_n-A_\infty^{(p)}\sim\delta^{-n},$$

$$c_n-2=-1+(-\lambda_1)^{p^{-n}}\sim\ln(-\lambda_1)p^{-n} \quad \text{for large } n. \tag{3.41}$$

Note also that the asymptotic scaling of the coupling-parameter sequence is governed only by the second CE, $\nu_2=p$, of the ''conjugate'' fixed map (3.38) for $p=3$ and of the zero-coupling fixed map (3.37) for $p=4$. Hence the critical scaling behavior of the coupling parameter near both ends becomes the same.

Figures 15(a) and 15(b) show three plots of $\lambda_{1,n}(A_\infty^{(p)},c)$ versus c for $n=1,2,3$ in the period-tripling ($p=3$) and period-quadrupling ($p=4$) cases, respectively. The critical asynchronous stability multipliers λ_1^* of Eq. (2.28) at both ends of the critical line segment can be easily obtained from Eq. (3.39). For $p=3$, $\lambda_1^*=\lambda^*(-\lambda^*)$ at the left (right) end (λ^* is the critical stability multiplier for the 1D case), while for $p=4$, $\lambda_1^*=\lambda^*$ at both ends. The slopes S_n of $\lambda_{1,n}$ at both ends also obey well the same one-term scaling law,

$$S_n=\left.\frac{\partial\lambda_{1,n}}{\partial c}\right|_{(A_\infty^{(p)},c^*)}\sim p^n \quad \text{for large } n, \tag{3.42}$$

where $c^*=c_l^*$ or c_r^* Hence the growth of S_n for large n is governed only by the second CE, ν_2 $(=p)$.

All interior points of the critical line segment become critical ones with $\lambda_1^*=0$, because at any interior point $\lambda_{1,n}$ converges to zero as $n\to\infty$. Hence the CB inside the critical

line segment becomes the same as that of the 1D map, as will be seen below. This kind of 1D-like CB is governed by the fixed maps with the same reduced coupling function $G^{*'}(x)=\frac{1}{2}f^{*'}(x)$, which have no relevant CE's.

For the dissipatively coupled case, the asynchronous Lyapunov exponent σ_1 is given by

$$\sigma_1(A,c)=\sigma_0(A)+\ln|1-c|, \tag{3.43}$$

where σ_0 is the 1D Lyapunov exponent of Eq. (3.18). In order to see the phase dynamics near the critical line segment, we fix the value of the nonlinearity parameter $A=A_\infty^{(p)}$. Then, the asynchronous Lyapunov exponent becomes $\sigma_1(A_\infty^{(p)},c)=\ln|1-c|$, because $\sigma_0(A_\infty^{(p)})=0$. Inside the critical line segment $(0<c<2)$, the synchronous quasiperiodic orbit on the $y=x$ symmetry line becomes a synchronous attractor with $\sigma_1<0$ [see Figs. 6(a) and 12(a)]. Note that the dynamics on the synchronous attractor is the same as that for the uncoupled 1D case. Hence the critical maps inside the critical line segment exhibit 1D-like CB. However, as the coupling parameter c passes through c_l^* or c_r^* the asynchronous Lyapunov exponent σ_1 of the synchronous quasiperiodic orbit increases from zero, and hence the coupling leads to desynchronization of the interacting systems. Thus the synchronous quasiperiodic orbit ceases to be an attractor outside the critical line segment, and new asynchronous attractors appear, as shown in Fig. 16.

We also study the scaling behavior of the asynchronous Lyapunov exponent σ_1 near both ends of the critical line segment. The asynchronous Lyapunov exponent near both ends becomes $\sigma_1\sim\epsilon$, where $\epsilon\equiv c-c^*$ ($c^*=c_l^*$ or c_r^*). As in the linearly coupled case, using the scaling theory, one can also obtain the scaling relation of σ_1, $\sigma_1\sim\epsilon^\eta$ with exponent $\eta=\ln p/\ln\nu_2=1$, where ν_2 $(=p)$ is the second CE of the fixed maps (3.37) and (3.38).

IV. EXTENSION TO MANY-COUPLED MAPS

In this section we study the CB of period p-tuplings in N $(N\geqslant 3)$ coupled 1D maps, in which the coupling extends to the Kth $\{1\leqslant K\leqslant (N/2)[(N-1)/2]$ for even (odd) $N\}$ neighbor(s) with equal strength. It is found that the CB depends on the range of coupling. In the global-coupling case, in which each 1D map is coupled to all the other 1D maps with equal strength, both the structure of the critical set and the CB are the same as those for the two-coupled case, irrespectively of N. However, for the cases of nonglobal couplings of shorter range, a significant change in the structure of the critical set may or may not occur according to whether the coupling is linear or not. As examples of the linear and nonlinear nonglobal couplings, we study the linearly and diffusively coupled, nearest-neighbor coupling cases, respectively. For the linearly coupled case, of the infinite number of period p-tupling routes for the global-coupling case, only the route ending at the zero-coupling critical point is left in the parameter plane. On the other hand, for the diffusively coupled case, one critical line segment constitutes the critical set, as in the globally coupled case.

A. Stability of periodic orbits in many-coupled maps

Consider N symmetrically coupled 1D maps with a periodic boundary condition,

$$\begin{aligned} T: x_m(t+1)&=F(\sigma^{m-1}\mathbf{x}(t))\\ &=F(x_m(t),x_{m+1}(t),\ldots,x_{m-1}(t)),\end{aligned}$$

$$m=1,\ldots,N \tag{4.1}$$

where N is a positive integer larger than or equal to 2, $\mathbf{x}=(x_1,\ldots,x_N)$, and σ is the cyclic permutation of $\mathbf{x}$ [i.e., $\sigma\mathbf{x}=(x_2,\ldots,x_1)$]. Here $x_m(t)$ is the state of the mth element at a discrete time t, and the periodic condition imposes $x_m(t)=x_{m+N}(t)$ for all m. Like the two-coupled case with $N=2$, the function F consists of two parts:

$$F(\mathbf{x})=f(x_1)+g(\mathbf{x}), \tag{4.2}$$

where f is an uncoupled 1D map with a quadratic maximum at $x=0$, and g is a coupling function. The uncoupled 1D map f satisfies the normalization condition (2.2), and the coupling function g obeys the condition

$$g(x,\ldots,x)=0 \quad \text{for any } x. \tag{4.3}$$

The N-coupled map T has a cyclic permutation symmetry,

$$\sigma^{-1}T\sigma(\mathbf{x})=T(\mathbf{x}) \quad \text{for all } \mathbf{x}, \tag{4.4}$$

where σ^{-1} is the inverse of σ. The set of all fixed points of σ forms a symmetry line on which

$$x_1=\cdots=x_N. \tag{4.5}$$

It follows from Eq. (4.4) that the cyclic permutation σ commutes with the map T, i.e., $\sigma T=T\sigma$. Hence the symmetry line becomes invariant under T, i.e., if a point $\mathbf{x}$ lies on the symmetry line, then its image $T(\mathbf{x})$ also lies on it. An orbit is called a synchronous orbit if it lies on the symmetry line, i.e., it satisfies

$$x_1(t)=\cdots=x_N(t)\equiv x(t) \quad \text{for all } t. \tag{4.6}$$

Otherwise, it is called an asynchronous orbit. Here we study only the synchronous orbits. They can be easily found from the uncoupled 1D map, $x(t+1)=f[x(t)]$, because of the condition (4.3).

Consider an element, say the mth element, in the N-coupled map T. Then the $(m\pm\delta)$th elements are called the δth neighbors of the mth element, where $1\leqslant\delta\leqslant(N/2)[(N-1)/2]$ for even (odd) N. If the coupling extends to the Kth neighbor(s), then the number K is called the range of coupling.

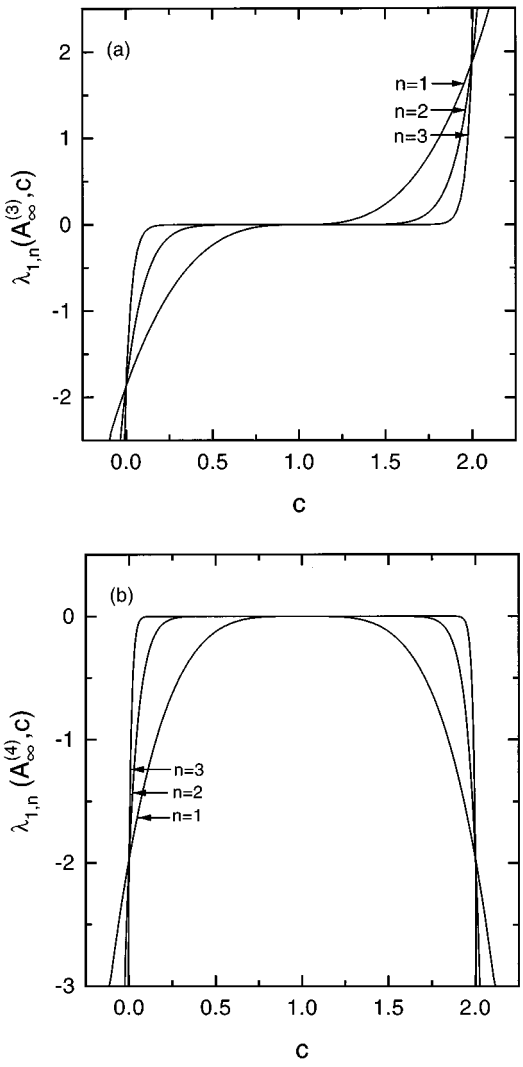

FIG. 15. Plots of the asynchronous stability multipliers $\lambda_{1,n}(A_\infty^{(p)},c)$ versus c for the synchronous orbits of period p^n ($n=1,2,3$) near the critical line for the (a) period-tripling ($p=3$) and (b) period-quadrupling ($p=4$) cases in two dissipatively coupled maps.

A general form of coupling for odd N ($N\geqslant 3$) is given by

$$g(x_1,\ldots,x_N)=\frac{c}{2K+1}\sum_{m=-K}^{K}[u(x_{1+m})-u(x_1)]$$
$$=c\left[\frac{1}{2K+1}\sum_{m=-K}^{K}u(x_{1+m})-u(x_1)\right],$$
$$K=1,\ldots,\frac{N-1}{2} \tag{4.7}$$

where c is a coupling parameter and u is a function of one variable. Here the coupling extends to the Kth neighbors with equal coupling strength, and the function g satisfies the condition (4.3). The extreme long-range interaction for $K=(N-1)/2$ is called a global coupling, for which the coupling function g becomes

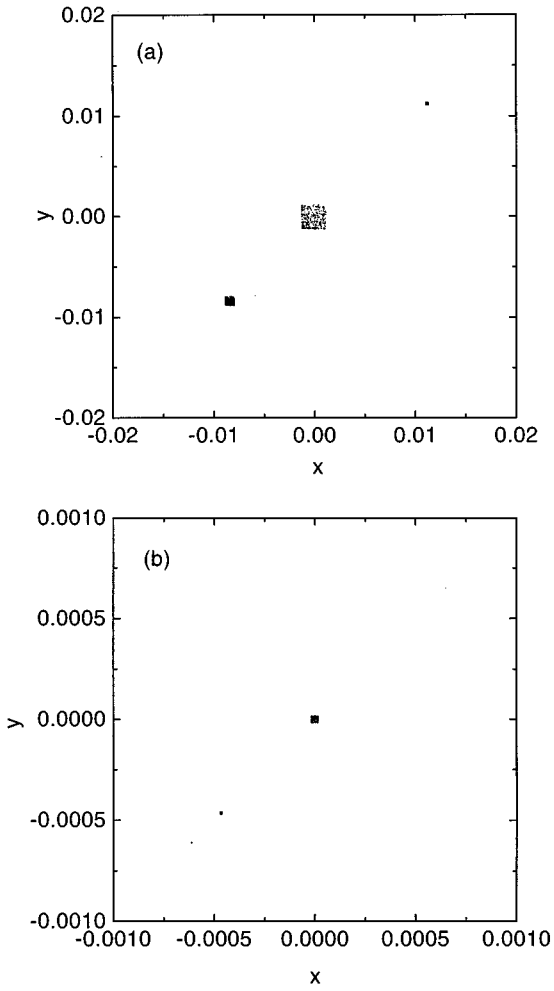

FIG. 16. Asynchronous attractors outside the critical line for (a) $c=-0.001\,5$ in the period-tripling case and (b) $c=-0.000\,1$ for the period-quadrupling case. For each case, the map is iterated 100 000 times to eliminate transients and the next 10 000 iterations are plotted.

$$g(x_1,\ldots,x_N)=\frac{c}{N}\sum_{m=1}^{N}[u(x_m)-u(x_1)]$$
$$=c\left[\frac{1}{N}N\sum_{m=1}^{N}u(x_m)-u(x_1)\right]. \tag{4.8}$$

This is a kind of mean-field coupling, in which each element is coupled to all the other elements with equal coupling strength. All the other couplings with $K<(N-1)/2$ (e.g., nearest-neighbor coupling with $K=1$) will be referred to as nonglobal couplings. The $K=1$ case for $N=3$ corresponds to both the global coupling and the nearest-neighbor coupling.

We next consider the case of even N ($N\geqslant 2$). The form of coupling of Eq. (4.7) holds for the cases of nonglobal couplings with $K=1,\ldots,(N-2)/2$ ($N\geqslant 4$). The global coupling for $K=N/2$ ($N\geqslant 2$) also has the form of Eq. (4.8), but it cannot have the form of Eq. (4.7), because there exists only one farthest neighbor for $K=N/2$, unlike the case of odd N. The $K=1$ case for $N=2$ also corresponds to the

nearest-neighbor coupling as well as to the global coupling, like the $N=3$ case.

The stability analysis of an orbit in many-coupled maps is conveniently carried out by Fourier transforming with respect to the discrete space $\{m\}$ [20]. Consider an orbit $\{x_m(t);m=1,\ldots,N\}$ of the N-coupled maps (4.1). The discrete spatial Fourier transform of the orbit is

$$\mathcal{F}[x_m(t)]\equiv\frac{1}{N}\sum_{m=1}^{N} e^{-2\pi imj/N}x_m(t)=\xi_j(t),$$

$$j=0,1,\ldots,N-1. \quad (4.9)$$

The Fourier transform $\xi_j(t)$ satisfies $\xi_j^*(t)=\xi_{N-j}(t)$ (* denotes complex conjugate), and the wavelength of a mode with index j is N/j for $j\leqslant N/2$ and $N/(N-j)$ for $j>N/2$.

To determine the stability of a synchronous orbit $[x_1(t)=\cdots=x_N(t)\equiv x(t)$ for all $t]$, we consider an infinitesimal perturbation $\{\delta x_m(t)\}$ to the synchronous orbit, i.e., $x_m(t)=x(t)+\delta x_m(t)$ for $m=1,\ldots,N$. Linearizing the N-coupled map (4.1) at the synchronous orbit, we obtain

$$\delta x_m(t+1)=f'(x(t))\delta x_m(t)+\sum_{l=1}^{N} G^{(l)}(x(t))\delta x_{l+m-1}, \quad (4.10)$$

where

$$G^{(l)}(x)\equiv\left.\frac{\partial g(x_1,\ldots,x_N)}{\partial x_l}\right|_{x_1=\cdots=x_N=x}. \quad (4.11)$$

Hereafter the functions $G^{(l)}$ will be called ''reduced'' coupling functions of $g(x_1,\ldots,x_N)$.

Let $\delta\xi_j(t)$ be the Fourier transform of $\delta x_m(t)$, i.e.,

$$\delta\xi_j=\mathcal{F}[\delta x_m(t)]=\frac{1}{N}\sum_{m=1}^{N} e^{-2\pi imj/N}\delta x_m,$$

$$j=0,1,\ldots,N-1. \quad (4.12)$$

Here $\delta\xi_0$ is the synchronous-mode perturbation, and all the other $\delta\xi_j$'s with nonzero indices j are the asynchronous-mode perturbations. Then the Fourier transform of Eq. (4.10) becomes

$$\delta\xi_j(t+1)=\left(f'(x(t))+\sum_{l=1}^{N} G^{(l)}(x(t))e^{2\pi i(l-1)j/N}\right)\times\delta\xi_j(t), \quad j=0,1,\ldots,N-1. \quad (4.13)$$

Note that all the modes $\delta\xi_j$ become decoupled for the synchronous orbit.

For a synchronous orbit with period q, its linear stability is determined by iterating the linearized map (4.13) q times:

$$\delta\xi_j(t+1)=\prod_{m=0}^{q-1}\left[f'(x(t+m))+\sum_{l=1}^{N} G^{(l)}(x(t+m))e^{2\pi i(l-1)j/N}\right]\times\delta\xi_j(t), \quad j=0,1,\ldots,N-1. \quad (4.14)$$

That is, the stability multipliers of the orbit are given by

$$\lambda_j=\prod_{t=0}^{q-1}\left(f'(x(t))+\sum_{l=1}^{N} G^{(l)}(x(t))e^{2\pi i(l-1)j/N}\right),$$

$$j=0,1,\ldots,N-1. \quad (4.15)$$

Here the first stability multiplier λ_0 is associated with the stability against the synchronous-mode perturbation, and hence it may be called the synchronous stability multiplier. On the other hand, all the other stability multipliers λ_j $(j\neq 0)$ are called the asynchronous stability multipliers, because they are associated with the stability against the asynchronous-mode perturbations.

A synchronous orbit becomes stable when it is stable against all the synchronous-mode and asynchronous-mode perturbations, i.e., the moduli of all stability multipliers are less than unity ($|\lambda_j|<1$ for $j=0,\ldots,N-1$). Hence the stable region of the synchronous orbit in the parameter plane is bounded by the synchronous and asynchronous bifurcation lines determined by the equations $\lambda_j=\pm 1$ for $j=0,\ldots,N-1$. When the $\lambda_0=1(-1)$ line is crossed, the synchronous orbit loses its stability via synchronous saddle-node (period-doubling) bifurcation. However, when the λ_j $(j\neq 0)=1(-1)$ line is crossed, it becomes unstable via asynchronous pitchfork (period-doubling) bifurcation.

It follows from Eq. (4.3) that

$$\sum_{l=1}^{N} G^{(l)}(x)=0. \quad (4.16)$$

Hence the synchronous stability multiplier λ_0 for $j=0$ becomes

$$\lambda_0=\prod_{t=0}^{q-1} f'(x(t)), \quad (4.17)$$

which is just the stability multiplier of the uncoupled 1D map. While there is no coupling effect on λ_0, the coupling generally affects asynchronous stability multipliers λ_j of $j\neq 0$. The effect of the coupling on the asynchronous stability multipliers depends on the range of coupling, as will be seen in the next two subsections.

B. Global-coupling case

In this subsection we study the CB of period p-tuplings in many-coupled maps with a global coupling. It is shown that both the structure of the critical set and the CB for the case of N globally coupled maps are the same as those for the case of two-coupled maps, independently of N.

In the case of the global coupling (4.8), the reduced coupling functions of Eq. (4.11) become

$$G^{(l)}(x)=\begin{cases}(1-N)G(x) & \text{for } l=1\\ G(x) & \text{for } l\neq 1,\end{cases} \tag{4.18}$$

where $G(x)=(c/N)u'(x)$. Substituting $G^{(l)}$'s into Eq. (4.15), we find that all the asynchronous stability multipliers are the same:

$$\lambda_1=\cdots=\lambda_{N-1}=\prod_{t=0}^{q-1}[f'(x(t))-NG(x(t))]$$
$$=\prod_{t=0}^{q-1}[f'(x(t))-cu'(x(t))]. \tag{4.19}$$

Hence there exist only two independent stability multipliers λ_0 and λ_1 $(=\lambda_1=\cdots=\lambda_{N-1})$ for the global-coupling case. Note also that the values of λ_0 and λ_1 are independent of N and they are the same as those of two-coupled maps. Thus the stability diagram of synchronous orbits of period p^n $(n=0,1,2,\ldots)$ in any N globally coupled maps becomes the same as that of the two-coupled maps. Consequently, the two-parameter scaling factors associated with scaling of the nonlinearity and coupling parameters are the same as those of the two-coupled maps, independently of N. That is, the CB of N globally coupled maps becomes the same as that for the case of the two-coupled maps, irrespectively of N, which is also shown below by a renormalization analysis.

We now follow the same procedure of Sec. II B and straightforwardly extend the renormalization results of the two coupled maps to many globally coupled maps. The rescaling operator B of Eq. (2.10) becomes αI for the case of N-coupled maps, where I is the $N\times N$ identity matrix. Applying the period p-tupling operator $\mathcal{N}$ of Eq. (2.9) to the N-coupled maps (4.1) n times, we obtain the n-times renormalized map T_n of the form

$$T_n: x_m(t+1)=F_n(x_m(t),x_{m+1}(t),\ldots,x_{m-1}(t))$$
$$=f_n(x_m(t))+g_n(x_m(t),x_{m+1}(t),\ldots,x_{m-1}(t)),$$
$$m=1,\ldots,N. \tag{4.20}$$

Here f_n and g_n are the uncoupled and coupling parts of the n-times renormalized function F_n, respectively. They satisfy the following recurrence equations:

$$f_{n+1}(x_1)=\alpha f_n^{(p)}\left(\frac{x_1}{\alpha}\right), \tag{4.21}$$

$$g_{n+1}(\mathbf{x})=\alpha F_n^{(p)}\left(\frac{\mathbf{x}}{\alpha}\right)-\alpha f_n^{(p)}\left(\frac{x_1}{\alpha}\right), \tag{4.22}$$

where

$$f_n^{(p)}(x_1)=f_n(f_n^{(p-1)}(x_1)), \tag{4.23}$$

$$F_n^{(p)}(\mathbf{x})=F_n(F_n^{(p-1)}(\mathbf{x}),F_n^{(p-1)}(\sigma\mathbf{x}),\ldots,F_n^{(p-1)}(\sigma^{N-1}\mathbf{x})), \tag{4.24}$$

and the rescaling factor is chosen to preserve the normalization condition $f_{n+1}(0)=1$, i.e., $\alpha=1/f_n^{(p-1)}(1)$. Then, the recurrence relations (4.21) and (4.22) define a renormalization operator $\mathcal{R}$ of transforming a pair of functions (f,g):

$$\begin{pmatrix}f_{n+1}\\ g_{n+1}\end{pmatrix}=\mathcal{R}\begin{pmatrix}f_n\\ g_n\end{pmatrix}. \tag{4.25}$$

A critical map with the nonlinearity and coupling parameters set to their critical values is attracted to a fixed map T^* under the iterations of the renormalization transformation $\mathcal{N}$:

$$T^*: x_m(t+1)=F^*(x_m(t),x_{m+1}(t),\ldots,x_{m-1}(t))$$
$$=f^*(x_m(t))$$
$$+g^*(x_m(t),x_{m+1}(t),\ldots,x_{m-1}(t)),$$
$$m=1,\ldots,N \tag{4.26}$$

where (f^*,g^*) is the fixed point of $\mathcal{R}$ with $\alpha=1/f^*(1)$. Since f^* is just the 1D fixed map, only the equation for the coupling fixed function g^* is left to be solved.

As in the two-coupled case, we construct a tractable recurrence equation for the reduced coupling function $G^{(l)}(x)$. That is, differentiating the recurrence equation (4.25) with respect to x_l $(l=2,\ldots,N)$ and setting $x_1=\cdots=x_N=x$, we obtain [21]

$$G_{n+1}^{(l)}(x)=F_{n,l}^{(p)}\left(\frac{x}{\alpha}\right)$$
$$=F_{n,l}^{(p-1)}\left(\frac{x}{\alpha}\right)f_n'\left(f_n^{(p-1)}\left(\frac{x}{\alpha}\right)\right)$$
$$+f_n^{(p-1)'}\left(\frac{x}{\alpha}\right)G_n^{(l)}\left(f_n^{(p-1)}\left(\frac{x}{\alpha}\right)\right)$$
$$+\sum_{m=1}^{N}F_{n,l-m+1}^{(p-1)}\left(\frac{x}{\alpha}\right)\left[G_n^{(m)}\left(f_n^{(p-1)}\left(\frac{x}{\alpha}\right)\right)\right.$$
$$\left.-G_n^{(l)}\left(f_n^{(p-1)}\left(\frac{x}{\alpha}\right)\right)\right],\quad l=2,\ldots,N \tag{4.27}$$

where $F_{n,m}^{(p)}(x)\equiv\partial F_n^{(p)}(\mathbf{x})/\partial x_m|_{x_1=\cdots=x_N=x}$ $(m=1,\ldots,N)$. Note that these reduced coupling functions satisfy the sum rule of Eq. (4.16) [i.e., $\Sigma_{l=1}^{N}G_n^{(l)}(x)=0$], and $G_n^{(l)}(x)=G_n^{(l+N)}(x)$ [or equivalently, $F_{n,m}^{(p)}(x)=F_{n,m+N}^{(p)}(x)$] due to the periodic condition.

In the global-coupling case, the initial reduced coupling functions $\{G^{(l)}(x)\}$ satisfy Eq. (4.18), i.e., there exists only one independent reduced coupling function $G(x)$. Then, it is easy to see that the successive images $\{G_n^{(l)}(x)\}$ of $\{G^{(l)}(x)\}$ under the transformation (4.27) also satisfy Eq. (4.18), i.e.,

$$G_n^{(2)}(x)=\cdots=G_n^{(N)}(x)\equiv G_n(x) \tag{4.28}$$

$$[\text{or equivalently, } F_{n,2}^{(p)}(x)=\cdots=F_{n,N}^{(p)}(x)\equiv F_n^{(p)}(x)]. \tag{4.29}$$

Consequently, there remains only one recurrence equation for the independent reduced coupling function $G(x)$:

$$G_{n+1}(x)=F_n^{(p)}\left(\frac{x}{\alpha}\right)$$
$$=F_n^{(p-1)}\left(\frac{x}{\alpha}\right)\left[f_n'\left(f_n^{(p-1)}\left(\frac{x}{\alpha}\right)\right)-NG_n\left(f_n^{(p-1)}\left(\frac{x}{\alpha}\right)\right)\right]$$
$$+f_n^{(p-1)'}\left(\frac{x}{\alpha}\right)G_n\left(f_n^{(p-1)}\left(\frac{x}{\alpha}\right)\right). \quad (4.30)$$

Then, together with Eq. (4.21), Eq. (4.30) defines a reduced renormalization operator $\tilde{\mathcal{R}}$ of transforming a pair of functions (f,G) such that $(f_{n+1},G_{n+1})=\tilde{\mathcal{R}}(f_n,G_n)$.

We look for fixed points (f^*,G^*) of $\tilde{\mathcal{R}}$ such that $(f^*,G^*)=\tilde{\mathcal{R}}(f^*,G^*)$. Here $f^*(x)$ is just the 1D fixed function. Only the equation for G^* is therefore left to be solved. Since the transformation (4.30) for G holds for any globally coupled map cases with $N\geqslant 2$, it can be regarded as a generalized version of Eq. (2.21) for the two-coupled case. Comparing the expression in Eq. (4.30) with that in Eq. (2.21), one can easily see that they are the same except for the factor N. Making a change of the independent reduced coupling function $G(x)\rightarrow(2/N)G(x)$ [equivalently, $F^{(p)}(x)\rightarrow(2/N)F^{(p)}(x)$], Eq. (4.30) is transformed into Eq. (2.21). Consequently, rescaling the solutions (2.26) for the two-coupled case with the scaling factor $2/N$, one can obtain the solutions for the case of N globally coupled maps:

$$G^*(x)=0 \quad \text{for all} \quad p, \quad (4.31a)$$

$$G^*(x)=\frac{1}{N}f^{*'}(x) \quad \text{for all} \quad p, \quad (4.31b)$$

$$G^*(x)=\frac{1}{N}[f^{*'}(x)-1] \quad \text{for all} \quad p, \quad (4.31c)$$

$$G^*(x)=\frac{1}{N}[f^{*'}(x)+1] \quad \text{for odd} \quad p, \quad (4.31d)$$

$$G^*(x)=\frac{2}{N}f^{*'}(x) \quad \text{for odd} \quad p. \quad (4.31e)$$

Thus there exist three (five) fixed points (f^*,G^*) of $\tilde{\mathcal{R}}$ for the case of even (odd) p, independently of N.

For the same reason as for the two-coupled maps [see Eq. (2.29)], the critical stability multipliers have the values of the stability multipliers of the fixed point of the fixed map T^*. From Eqs. (4.17) and (4.19), we obtain two independent critical stability multipliers λ_0^* and λ_1^*:

$$\lambda_0^*=f^{*'}(\hat{x}), \quad \lambda_1^*=f^{*'}(\hat{x})-NG^*(\hat{x}), \quad (4.32)$$

where $\hat{x}$ is the fixed point of the 1D fixed function [i.e., $\hat{x}=f^*(\hat{x})$] and λ_0^* is just the critical stability multiplier λ^* of the uncoupled 1D map. Substituting G^*'s into Eq. (4.32), we obtain the same critical asynchronous stability multipliers λ_1^* as in the case of two-coupled maps, as listed in Table VIII.

Consider an infinitesimal perutrbation (h,Φ) to a fixed point (f^*,G^*) of the reduced renormalization operator $\tilde{\mathcal{R}}$.

TABLE VIII. Independent reduced coupling fixed functions $G^*(x)$, relevant CE's ν, and independent critical asynchronous stability multipliers λ_1^* in all the period p-tupling cases are shown for the case of N globally coupled maps. The first three for $G^*(x)$ exist for all p, whereas the last two exist only for odd p. Here α and λ^* are the orbital scaling factor and the critical stability multiplier for the 1D case, respectively. Note that ν and λ_1^* for each $G^*(x)$ are also the same as those for the two-coupled case, independently of N.

$G^*(x)$	ν	λ_1^*
0	α, p	λ^*
$\frac{1}{N}f^{*\prime}$	nonexistent	0
$\frac{1}{N}[f^{*\prime}(x)-1]$	p	1
$\frac{1}{N}[f^{*\prime}(x)+1]$	p	-1
$\frac{2}{N}f^{*\prime}(x)$	α, p	$-\lambda^*$

Linearizing $\tilde{\mathcal{R}}$ at the fixed point, we obtain the recurrence equation for the evolution of (h,Φ), $(h_{n+1},\Phi_{n+1})=\tilde{\mathcal{L}}(h_n,\Phi_n)$. As in the two-coupled case, the linearized operator $\tilde{\mathcal{L}}$ also has a semiblock form [i.e., $h_{n+1}(x)=[\tilde{\mathcal{L}}_1h_n](x)$ and $\Phi_{n+1}(x)=[\tilde{\mathcal{L}}_2\Phi_n](x)+[\tilde{\mathcal{L}}_3h_n](x)$]. It follows from the reducibility of $\tilde{\mathcal{L}}$ into a semiblock form that one can find eigenvalues of $\tilde{\mathcal{L}}_1$ and $\tilde{\mathcal{L}}_2$ separately and then they give the whole spectrum of $\tilde{\mathcal{L}}$.

All the fixed points (f^*,G^*) have a common relevant eigenvalue δ of $\tilde{\mathcal{L}}_1$ (i.e., the relevant eigenvalue for the case of the uncoupled 1D maps) associated with the critical scaling of the nonlinearity parameter of the uncoupled 1D map. However, the relevant CE's of $\tilde{\mathcal{L}}_2$, associated with the critical scaling of the coupling parameter, depend on the kind of the fixed points, as in the case of the two-coupled maps. Consider an infinitesimal perturbation Φ to a fixed point G^* of the recurrence equation (4.30). Linearizing Eq. (4.30) at the fixed point G^*, we obtain an equation for the evolution of Φ [i.e., $\Phi_{n+1}(x)=\tilde{\mathcal{L}}_2\Phi_n(x)$]. Note again that Eq. (4.30) is transformed into the recurrence equation (2.21) for the two-coupled case under a mere scale change of the independent reduced coupling function $G(x)\rightarrow(2/N)G(x)$. Consequently, the CE equation [i.e., $\tilde{\mathcal{L}}_2\Phi^*(x)=\nu\Phi^*(x)$] for the case of N globally coupled maps becomes the same as that for the case of two-coupled maps, independently of N. Then, following the same procedure of Sec. II B, one can obtain the same CE's as those for the case of two-coupled maps, as listed in Table VIII.

C. Nonglobal-coupling cases

In this subsection, we choose $f(x)=1-Ax^2$ as the uncoupled 1D map and study the CB of the period p-tuplings for the nonglobal-coupling cases. A significant change in the structure of the critical set may or may not occur according to whether the coupling is linear or not. As examples of the

linear and nonlinear nonglobal couplings, we study the linearly and diffusively coupled, nearest-neighbor coupling cases, respectively. For the linearly coupled case, only the zero-coupling critical point is left in the parameter plane, which is in contrast to the global-coupling case. On the other hand, for the diffusively coupled case, one critical line segment constitutes the critical set, as in the global-coupling case.

Consider a nonglobal coupling of the form (4.7) and define

$$G(x)\equiv\frac{c}{2K+1}u'(x), \tag{4.33}$$

where $1\leqslant K\leqslant[(N-2)/2][(N-3)/2]$ for even (odd) N larger than 3. Then we have

$$G^{(l)}(x)=\begin{cases}-2KG(x) & \text{for } l=1\\ G(x) & \text{for } 2\leqslant l\leqslant 1+K \text{ or}\\ & \text{for } N+1-K\leqslant l\leqslant N\\ 0 & \text{otherwise.}\end{cases} \tag{4.34}$$

Substituting $G^{(l)}$'s into Eq. (4.15), we find that each stability multiplier λ_j (associated with the stability against the jth-mode perturbation) is given by

$$\lambda_j=\prod_{t=0}^{q-1}[f'(x(t))-S_N(K,j)cu'(x(t))], \tag{4.35}$$

where

$$S_N(K,j)\equiv\frac{4}{2K+1}\sum_{k=1}^{K}\sin^2\frac{\pi jk}{N}=1-\frac{\sin(2K+1)(\pi j/N)}{(2K+1)\sin(\pi j/N)}. \tag{4.36}$$

Hence, unlike the global-coupling case [see Eq. (4.19)], the stability multipliers vary depending on the coupling range K as well as on the mode number j. Since $S_N(K,j)=S_N(K,N-j)$, the stability multipliers satisfy

$$\lambda_j=\lambda_{N-j},\quad j=0,1,\ldots,N-1. \tag{4.37}$$

Thus it is sufficient to consider only the case of $0\leqslant j\leqslant(N/2)$ $[(N-1)/2]$ for even (odd) N. Comparing the expression in Eq. (4.35) with that in Eq. (4.19) for $j\neq 0$, one can easily see that they are the same except for the factor $S_N(K,j)$. Consequently, making a change of the coupling parameter $c\to c/S_N(K,j)$, the stability multiplier λ_j for the nonglobal-coupling case of range K becomes the same as that for the global-coupling case.

For each mode with nonzero index j, we consider a region in the parameter plane, in which a synchronous orbit is stable against the perturbations of both modes with indices 0 and j. This stable region is bounded by four bifurcation curves determined by the equations $\lambda_0=\pm 1$ and $\lambda_j=\pm 1$, and it will be denoted by U_N. For the case of global coupling, those stable regions coincide, irrespectively of N and j, because all the asynchronous stability multipliers λ_j $(j\neq 0)$ are the same, independently of N. The stable region for this global-coupling case will be denoted by U_G. Note that U_G itself is just the stability region of the synchronous orbit, irrespectively of N, because the synchronous orbit is stable against the perturbations of all the synchronous and asynchronous modes in the region U_G.

However, the stable regions U_N vary depending on the coupling range K and the mode number j for the nonglobal-coupling cases, i.e., $U_N=U_N(K,j)$. To find the stability region of a synchronous orbit in an N-coupled map with a given K, one may start with the stability region U_G for the global-coupling case. Rescaling the coupling parameter c by a scaling factor $1/S_N(K,j)$ for each nonzero j, the stable region U_G is transformed into a stable region $U_N(K,j)$. Then the stability region of the synchronous orbit is given by the intersection of all such stable regions U_N. A significant change in the stability diagram of the synchronous orbits of period p^n $(n=0,1,2,\ldots)$ may or may not occur according to whether the coupling is linear or not, as will be seen below.

As the first example, we study the linearly coupled, nearest-neighbor coupling case with $K=1$, in which the coupling function is

$$g(x_1,\ldots,x_N)=\frac{c}{3}(x_2+x_N-2x_1)\quad\text{for } N\geqslant 3. \tag{4.38}$$

This kind of coupling can be regarded as a generalized version of Eq. (3.1) for the linearly coupled case for $N=2$. (Note that as mentioned above, the cases of $N=2$ and 3 correspond to the global-coupling case.) For $K=1$, the scaling factor $1/S_N(K,j)$ of Eq. (4.36) becomes

$$S_N(1,j)=\frac{4}{3}\sin^2\left(\frac{\pi j}{N}\right). \tag{4.39}$$

This scaling factor $1/S_N(1,j)$ has its minimum value $\frac{3}{4}\{3/[4\cos^2(\pi/2N)]\}$ at $j_{\min}=(N/2)[(N-\frac{1}{2})]$ for even (odd) N. We also note that the minimum value for odd N depends on N, but as $N\to\infty$ it converges to the minimum value for the case of even N.

Rescaling the coupling parameter c with the scaling factor $1/S_N(1,j)$, the stability region U_G for the $N=2$ and 3 cases of global coupling is transformed into the region $U_N(1,j)$ for $N>3$. Then, as a result of the intersection of all such regions $U_N(1,j)$, only the region $U_N(1,j_{\min})$ including a $c=0$ line segment is left as the stability region of a synchronous orbit. Consequently, of the infinite number of period p-tupling routes for the global-coupling case, only the Z_p route ending at the zero-coupling critical point $(A_\infty^{(p)},0)$ remains. Thus only the zero-coupling point is left as a critical point in the parameter plane. An example for the period-tripling case with $p=3$ is shown in Fig. 17. The largest stability region corresponds to the stability region for the $N=2$ and 3 cases of the global coupling, while the smallest one corresponds to that for the case of even N $(N>2)$. Between them, there exist stability regions for the case of odd N $(N>3)$ (e.g., see the $N=5$ case in Fig. 17).

We now examine the CB near the zero-coupling critical point for the case of the linearly coupled, nearest-neighbor

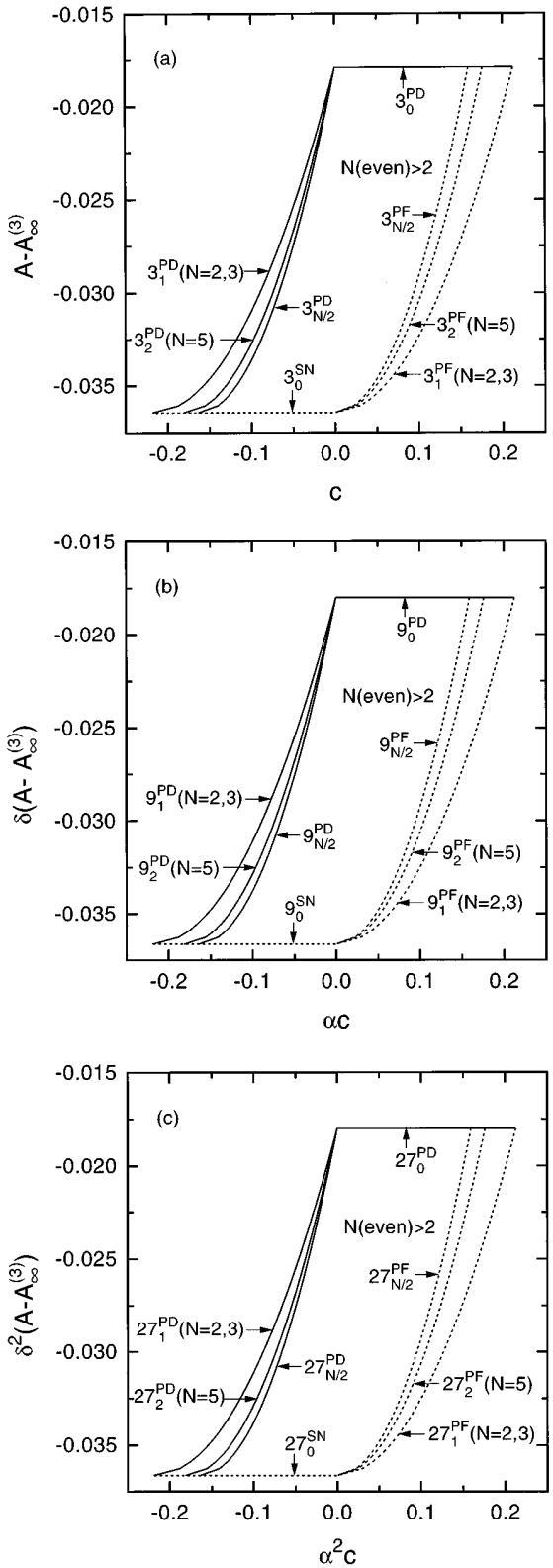

FIG. 17. Stable regions of the synchronous 3^n-periodic orbits of level $n=1,2,3$ in N ($N=2,3,4,\ldots$) coupled 1D maps for the linearly coupled, nearest-neighbor coupling case with $K=1$. The cases of $n=1$, 2, and 3 are shown in (a), (b), and (c), respectively. The symbols q_j^{PD}, q_j^{SN}, and q_j^{PF} with $j=0$ and $j_{\min}$ represent the period-doubling, saddle-node, and pitchfork bifurcation lines associated with the stability of a synchronous orbit of period q against the perturbation of the jth mode. The scaling factors used in (b) and (c) are $\delta=55.247\,026$ and $\alpha=-9.277\,341$. For other details, see the text.

coupling. Consider a self-similar sequence of parameters (A_n,c_n), at which the synchronous orbit of level n has some given stability multipliers, in the Z_p route for the global-coupling case. Rescaling the coupling parameter with the factor $1/S_N(1,j_{\min})$, this sequence is transformed into a self-similar one for the case of the linearly coupled, nearest-neighbor coupling. Thus the ''width'' of each stability region in the Z_p route for the case of the global coupling is reduced to that for the case of the linearly coupled, nearest-neighbor coupling by the scaling factor $1/S_N(1,j_{\min})$, while the ''heights'' of all stable regions in the Z_p route remain unchanged [22]. It is therefore obvious that the critical scaling behavior near the zero-coupling critical point for the case of the linearly coupled, nearest-neighbor coupling is the same as that for the global-coupling case. That is, the height and width h_n and w_n of the stability region of level n geometrically contract in the limit of large n,

$$h_n\sim\delta^{-n},\quad w_n\sim\alpha^{-n}\quad\text{for large } n, \tag{4.40}$$

where δ and α are the scaling factors of the nonlinearity and coupling parameters, respectively. As an example, see again Fig. 17 and note that Figs. 17(a), 17(b), and 17(c) nearly coincide near the zero-coupling critical point except for small numerical differences.

The results of the linearly coupled, nearest-neighbor coupling with $K=1$ extend to all the other linearly coupled, nonglobal-coupling cases with $1<K<(N/2)[(N-1)/2]$ for even (odd) N. For each nonglobal-coupling case with $K>1$, we first consider a mode with index $j_{\min}$ for which the scaling factor $1/S_N(K,j)$ becomes the smallest one. Here the value of $j_{\min}$ varies depending on the range K. Like the $K=1$ case, only the region $U_N(K,j_{\min})$ including a $c=0$ line segment is left as the stability region of a synchronous orbit. Consequently, only the zero-coupling point remains as a critical point in the parameter plane, and the CB near the zero-coupling critical point is also the same as that for the global-coupling case.

Finally, as an example of the nonlinear coupling, we study the diffusively coupled, nearest-neighbor coupling case with $K=1$, in which the coupling function is given by

$$g(x_1,\ldots,x_N)=\frac{c}{3}[f(x_2)+f(x_N)-2f(x_1)]\quad\text{for } N\geqslant 3. \tag{4.41}$$

This kind of coupling can be regarded as a generalized version of Eq. (3.30) for the dissipatively coupled case for $N=2$. For this diffusively coupled case, the stability multipliers of Eq. (4.35) for a synchronous q-periodic orbit of level n ($q=p^n$) become

$$\lambda_j=[1-cS_N(1,j)]^q\lambda_0. \tag{4.42}$$

Like the linearly coupled case, rescaling the coupling parameter c with the minimum scaling factor $1/S_N(1,j_{\min})$, each stability region U_G of level n for the global-coupling case is transformed into the stability region [i.e., the region $U_N(1,j_{\min})$] of level n for the diffusively coupled case. The stability region $U_N(1,j_{\min})$ is bounded by four bifurcation curves determined by the equations $\lambda_j=\pm 1$ for $j=0,j_{\min}$. An infinite sequence of such stability regions converges to a

critical line segment joining two points c_l^* $(=0)$and c_r^* $[=2/S_N(1,j_{\min})]$ on the $A=A_\infty^{(p)}$ line. Consequently, one critical line segment constitutes the critical set, like the global-coupling case. An example for the period-tripling case for even N $(N>2)$ is shown in Fig. 18.

As shown above, the stability diagram for the diffusively coupled case is essentially the same as that for the globally coupled case, except for the scale in the coupling parameter c. Hence the critical scaling behavior of the nonlinearity and coupling parameters and so on becomes the same as that for the global-coupling case (for details on the CB, refer to Sec. III B). Finally, we briefly discuss the critical asynchronous stability multipliers. At the zero-coupling critical point $(A_\infty^{(p)},0)$ and interior critical points, they are the same as those for the global-coupling case [i.e., $\lambda_1^*=\cdots=\lambda_{N-1}^*=\lambda_0^*$ at $(A_\infty^{(p)},0)$, and $\lambda_1^*=\cdots=\lambda_{N-1}^*=0$ at interior critical points]. However, at the right end $(A_\infty^{(p)},c_r^*)$, the critical asynchronous stability multiplier for $j=j_{\min}$ is given by $\lambda_{j_{\min}}^*=\lambda_0^*$ (even q) and $-\lambda_0^*$ (odd q), but all other λ_j^*'s $(j\neq j_{\min})$ are zero, which is somewhat different from that for the global-coupling case [i.e., $\lambda_1^*=\cdots=\lambda_{N-1}^*=\lambda_0^*$ (even q) and $-\lambda_0^*$ (odd q)]. Like the linearly coupled case, the results for the diffusively coupled, nearest-neighbor coupling case with $K=1$ can also be extended to all the other diffusively coupled, nonglobal-coupling cases with $1<K<(N/2)[(N-1)/2]$ for even (odd) N.

V. SUMMARY

The CB's of all period p-tuplings $(p=2,3,4,\ldots)$ are studied in N $(N=2,3,4,\ldots)$ symmetrically coupled 1D maps. The two-coupled case with $N=2$ is first investigated by a renormalization method. We find three (five) kinds of fixed points of the renormalization operator and their relevant CE's associated with coupling perturbations for the case of even (odd) p. We next consider two kinds of couplings, linear and nonlinear couplings. As examples of the linear- and nonlinear-coupling cases, we study the linearly and dissipatively coupled maps, respectively, and confirm the renormalization results. The structure of the critical set varies depending on the nature of coupling. For the linearly coupled case, an infinite number of the critical line segments, together with the zero-coupling critical point, constitute the critical set, while for the dissipatively coupled case, the critical set consists of only one critical line segment. The CB also depends on the position on the critical set. For even (odd) p, three (four) kinds of fixed points govern the CB for the linearly coupled case, while only two (three) kinds of fixed points govern the CB for the dissipatively coupled case. Finally, the results of the two-coupled maps are extended to many-coupled maps with $N\geqslant 3$, in which the CB depends on the range of coupling. In the global-coupling case, both the structure of the critical set and the CB are the same as those of the two-coupled case, independently of N. However, for the nonglobal-coupling case, a significant change in the structure of the critical set may or may not occur according to whether the coupling is linear or not. For the linearly coupled case, of the infinite number of period p-tupling routes for the global-coupling case, only the route ending at the zero-coupling critical point is left in the parameter plane. On the other hand, for the diffusively coupled case, one critical line segment constitutes the critical set, as in the globally coupled case.

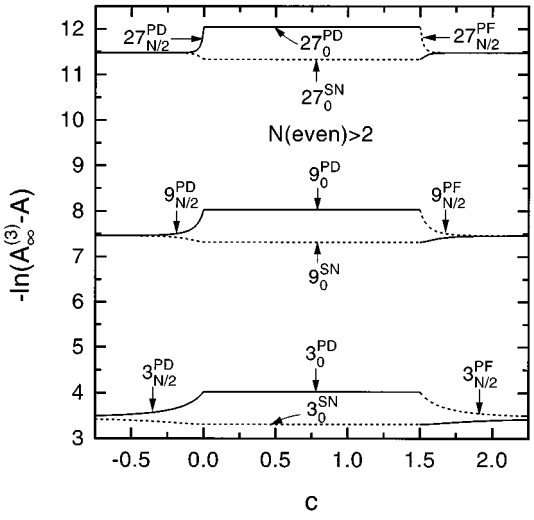

FIG. 18. Stable regions of the synchronous 3^n-periodic orbits of level $n=1,2,3$ in even-N- $(N>2)$ coupled 1D maps for the diffusively coupled, nearest-neighbor coupling case with $K=1$. The symbols q_j^{PD}, q_j^{SN}, and q_j^{PF} with $j=0$ and $j_{N/2}$ represent the period-doubling, saddle-node, and pitchfork bifurcation lines associated with the stability of a synchronous orbit of period q against the perturbation of the jth mode.

ACKNOWLEDGMENTS

This work was supported by the Basic Science Research Institute Program, Ministry of Education, Korea, Project No. BSRI-95-2401. The author thanks Professor R. Fox for his hospitality during a visit to the Georgia Institute of Technology.

[1] N. Metropolis, M. L. Stein, and P. R. Stein, J. Comb. Theor. **15**, 25 (1973).
[2] B. Derrida, A. Gervois, and Y. Pomeau, J. Phys. A **12**, 269 (1979).
[3] M. J. Feigenbaum, J. Stat. Phys. **19**, 25 (1978); **21**, 669 (1979).
[4] B. Hu and I. I. Satija, Phys. Lett. **98A**, 143 (1983).
[5] J.-P. Eckmann, H. Epstein, and P. Wittwer, Commun. Math. Phys. **93**, 495 (1984).
[6] W.-Z. Zeng and B.-L. Hao, Commun. Theor. Phys. **3**, 283 (1984).
[7] P. R. Hauser, C. Tsallis, and E. M. F. Curado, Phys. Rev. A **30**, 2074 (1984).

[8] S.-J. Chang and J. McCown, Phys. Rev. A **31**, 3791 (1985).
[9] R. Delbourgo, W. Hart, and B. G. Kenny, Phys. Rev. A **31**, 514 (1985); R. Delbourgo and B. G. Kenny, *ibid.* **33**, 3292 (1986).
[10] V. Urumov and L. Kocarev, Phys. Lett. A **144**, 220 (1990).
[11] K. Kaneko, in *Formation, Dynamics and Statistics of Patterns*, edited by K. Kawasaki, M. Suzuki, and A. Onuki (World Scientific, Singapore, 1990), pp. 1–54.
[12] S. Kuznetsov, Radiophys. Quantum Electron. **28**, 681 (1985); H. Kook, F. H. Ling, and G. Schmidt, Phys. Rev. A **43**, 2700 (1991).
[13] S.-Y. Kim and H. Kook, Phys. Rev. A **46**, R4467 (1992); Phys. Lett. A **178**, 258 (1993); Phys. Rev. E **48**, 785 (1993); S.-Y. Kim, *ibid.* **49**, 1745 (1994).
[14] S.-Y. Kim, Phys. Rev. E **52**, 1206 (1995).
[15] J. Gukenheimer and P. Holmes, *Nonlinear Oscillations, Dynamical Systems, and Bifurcations of Vector Fields* (Springer-Verlag, New York, 1983), Sec. 3.5.
[16] In deriving Eq. (2.21), we use the relation $F_{n,1}^{(p)}(x)+F_{n,2}^{(p)}(x)=f_n^{(p)'}(x)$, where $F_{n,1}^{(p)}(x)\equiv\partial F_n^{(p)}(x,y)/\partial x|_{y=x}$ and $F_{n,2}^{(p)}(x)\equiv\partial F_n^{(p)}(x,y)/\partial y|_{y=x}$.
[17] One can obtain Eqs. (2.24) and (2.40) by induction. Assume that a period p-tupling case satisfies Eqs. (2.24) and (2.40). Then, it follows from the assumption that the next period $(p+1)$-tupling also satisfies Eqs. (2.24) and (2.40). Moreover, one can easily show that the lowest even and odd cases, $p=2,3$, satisfy Eqs. (2.24) and (2.40). Consequently, Eqs. (2.24) and (2.40) are valid for all period p-tupling cases.
[18] S.-Y. Kim, Phys. Rev. E **50**, 4237 (1994).
[19] J.-M. Mao and B. Hu, J. Stat. Phys. **46**, 111 (1987); Int. J. Mod. Phys. B **2**, 65 (1988); C. Reick, Phys. Rev. A **45**, 777 (1992).
[20] I. Waller and R. Kapral, Phys. Rev. A **30**, 2047 (1984).
[21] In deriving Eq. (4.27), we use the relation $\Sigma_{l=1}^{N}F_{n,l}^{(p)}=f_n^{(p)'}(x)$, where $F_{n,l}^{(p)}(x)\equiv\partial F_n^{(p)}(\mathbf{x})/\partial x_l|_{x_1=\cdots=x_N=x}$ $(l=1,\ldots,N)$.
[22] We define the ''height'' h_n of the stable region of level n in the Z_p route as the length of the $c=0$ line segment inside the stable region. The ''width'' w_n is also defined as the length of the boundary line segment associated with the synchronous period-doubling bifurcation (i.e., the curve determined by the equation $\lambda_{0,n}=-1$).